Dinocyst assemblages and water surface conditions in the Sea of Marmara during MIS 6 and 5 from two long cores

S.A.G. Leroy, P. Henry, F. Marret, Christine Paillès, L. Licari, J. Kende, F. Rostek, Edouard Bard

▶ **To cite this version:**

S.A.G. Leroy, P. Henry, F. Marret, Christine Paillès, L. Licari, et al.. Dinocyst assemblages and water surface conditions in the Sea of Marmara during MIS 6 and 5 from two long cores. Quaternary Science Reviews, 2023, 314, pp.108229. 10.1016/j.quascirev.2023.108229 . hal-04227584

HAL Id: hal-04227584
https://hal.science/hal-04227584

Submitted on 3 Oct 2023

HAL is a multi-disciplinary open access archive for the deposit and dissemination of scientific research documents, whether they are published or not. The documents may come from teaching and research institutions in France or abroad, or from public or private research centers.

L'archive ouverte pluridisciplinaire **HAL**, est destinée au dépôt et à la diffusion de documents scientifiques de niveau recherche, publiés ou non, émanant des établissements d'enseignement et de recherche français ou étrangers, des laboratoires publics ou privés.

Quaternary Science Reviews

Dinocyst assemblages and water surface conditions in the Sea of Marmara during MIS 6 and 5 from two long cores

--Manuscript Draft--

Manuscript Number:	
Article Type:	Research Paper
Keywords:	Dinocysts, MIS 6 and 5, Marmara Sea, connection, sea level, sapropel
Corresponding Author:	Suzanne A.G. Leroy FRANCE
First Author:	Suzanne A.G. Leroy
Order of Authors:	Suzanne A.G. Leroy
	Pierre Henry
	fabienne Marret-Davies
	Christine Pailles
	Laetitia Licari
	julia kende
	frauke rostek
	edouard bard
Abstract:	The Sea of Marmara is the connection between the vast Black Sea-Caspian Sea basin (Pontocaspian) and the Global Ocean via the Mediterranean Sea. Its water levels and water conditions has widely varied over times. Combining two cores in the Sea of Marmara (Turkey) and using organic-walled dinoflagellate cysts as the main proxy (allied to alkenones, diatoms and benthic foraminifera), allow qualitatively reconstructing water conditions during Marine Isotopic Stage (MIS) 6 and 5. A clear main marine phase is illustrated in MIS 5e. A minor marine phase occurred during MIS 5c, mostly supported by alkenone data. The rest of the record indicates brackish Pontocaspian conditions, with more Spiniferites inaequalis in MIS 6 and more S. cruciformisin MIS 5. An earlier initial marine flooding in the Marmara Sea (MIS 6/MIS 5) in comparison to the Black Sea was highlighted on the base of difference in terrestrial vegetation reconstructed from pollen analyses in the same Marmara cores. Understanding the hydrologic evolution of the Sea of Marmara during MIS 5 implies taking into account the consequences of the disconnection of the Black Sea at the Bosphorus on the hydrodynamics and sediment transport processes in the Dardanelles Straight. The sapropels of the Marmara Sea form when marine water penetrates at depth from the Aegean Sea. Combining surface water proxies with benthic foraminifera (shells and inner organic lining), it suggests that the sapropels over time formed under decreasing anoxic conditions. A comparison between the two cores suggests anoxia did not rise up to 291 m water depth.
Suggested Reviewers:	Lyudmila Shumilovskikh University of Göttingen lshumil@gwdg.de she has published a dinocyst diagram in the Black Sea covering part of MIS5e
	Katarina Kouli National and Kapodistrian University of Athens akouli@geol.uoa.gr she has published a dino diagram from the G of Corinth with similar assemblages to the Marmara Sea
	Laurent Londeix University of Bordeaux l.londeix@epoc.u-bordeaux1.fr

Powered by Editorial Manager® and ProduXion Manager® from Aries Systems Corporation

Manuscript File Click here to view linked References

22/03/2023

Dinocyst assemblages and water surface conditions in the Sea of Marmara during MIS 6 and 5 from two long cores

Leroy S.A.G. [1-2-3-*], Henry P. [1], Marret F. [3], Pailles C. [1], Licari L. [1], Kende J. [1], Rostek F. [1], Bard E. [1]

1 Aix Marseille Univ, CNRS, IRD, INRAE, Coll France, CEREGE, Aix-en-Provence, France, suzleroy@hotmail.com, henry@cerege.fr, pailles@cerege.fr, licari@cerege.fr, jj.kende@gmail.com, rostek@cerege.fr, bard@cerege.fr

2 Aix Marseille Univ, CNRS, Minist. Culture & Com., LAMPEA, 13094 Aix-en-Provence, France

3 School of Environmental Sciences, University of Liverpool, L69 7ZT Liverpool, UK, fmarret@liverpool.ac.uk

** Corresponding author*

Abstract

The Sea of Marmara is the connection between the vast Black Sea-Caspian Sea basin (Pontocaspian) and the Global Ocean via the Mediterranean Sea. Its water levels and water conditions has widely varied over times. Combining two cores in the

Sea of Marmara (Turkey) and using organic-walled dinoflagellate cysts as the main proxy (allied to alkenones, diatoms and benthic foraminifera), allow qualitatively reconstructing water conditions during Marine Isotopic Stage (MIS) 6 and 5. A clear main marine phase is illustrated in MIS 5e. A minor marine phase occurred during MIS 5c, mostly supported by alkenone data. The rest of the record indicates brackish Pontocaspian conditions, with more *Spiniferites inaequalis* in MIS 6 and more *S. cruciformis* in MIS 5.

An earlier initial marine flooding in the Marmara Sea (MIS 6/MIS 5) in comparison to the Black Sea was highlighted on the base of difference in terrestrial vegetation reconstructed from pollen analyses in the same Marmara cores. Understanding the hydrologic evolution of the Sea of Marmara during MIS 5 implies taking into account the consequences of the disconnection of the Black Sea at the Bosphorus on the hydrodynamics and sediment transport processes in the Dardanelles Straight.

The sapropels of the Marmara Sea form when marine water penetrates at depth from the Aegean Sea. Combining surface water proxies with benthic foraminifera (shells and inner organic lining), it suggests that the sapropels over time formed under decreasing anoxic conditions. A comparison between the two cores suggests anoxia did not rise up to 291 m water depth.

Key words

Dinocysts, MIS 6 and 5, Marmara Sea, connection, sea level, sapropel

1 Introduction

The Sea of Marmara (SoM) is a gateway between the Mediterranean Sea and the Black Sea in Turkey, and has experienced water-level fluctuations and hydrological variations during the late Quaternary, which were mainly controlled by bedrock sills at the Marmara Sea exit of Çanakkale Strait (Dardanelles) and the Black Sea entrance of the Istanbul (Bosphorus) Strait, respectively. The variations in water depths of these sills were possibly governed by longer-term vertical displacements related to tectonics and erosion/sedimentation balance due to sea-level changes and water exchanges between the Black and Aegean seas, or between the Ponto-Caspian ensemble and the Global Ocean (Yaltırak, 2002; Gökaşan et al., 2008, Çağatay et al., 2009, 2019; Vidal et al., 2010; Eriş et al., 2011) (Fig. 1). The SoM is indeed a highly seismic area as it is located on the western end of the North Anatolian Fault; however, tectonics are mainly significantly affecting sea levels only in the long term. At the scale of the last climatic cycle, global ocean level change is the main factor controlling the water level in the SoM. For the last interglacial (Marine Isotope Stage 5, MIS 5), decreasing water level maxima are noted along the successive three warm stages: MIS 5e, 5c and 5a (Rohling et al., 2021). Moreover, the Black Sea level should be considered as another crucial influence on water level in the SoM, evidenced as the melting of the Eurasian icecap and the subsequent evacuation of the freshwater along large rivers flowing into the Black Sea (Tudryn et al., 2016) and, at times, the outflow from the Caspian Sea via the Manych Passage (Chepalyga, 2007). The SoM is the outlet of all the Pontocaspian basins (as far as the Tien-Shan via the Syr-Darya and the Chu River and the Pamir-Indu-Kush via the Amu-Darya) and hence this inland sea is the receptacle of the history of a large geographical area (Fig. 1). Thus, the water level

history of the SoM is quite complex (local, regional and global forcing) and its insight clearly has an extra-regional relevance. Its history starts to be well-known for the Last Glacial Maximum and the Holocene, but it remains much less clear before (Leroy et al., 2020; Eriş et al., 2007, 2011; Çağatay et al., 2009, 2015a). Moreover, the SoM forms sapropels under certain conditions. They are dark and finely laminated sediment rich in organic matter and are important to study as they consist of layers where carbon can be locked away from oxidation, thus contributing to the C cycle. In the Mediterranean Sea, enhanced marine productivity increases organic matter degradation and anoxia (Rohling et al., 2015; Zwiep et al., 2018).

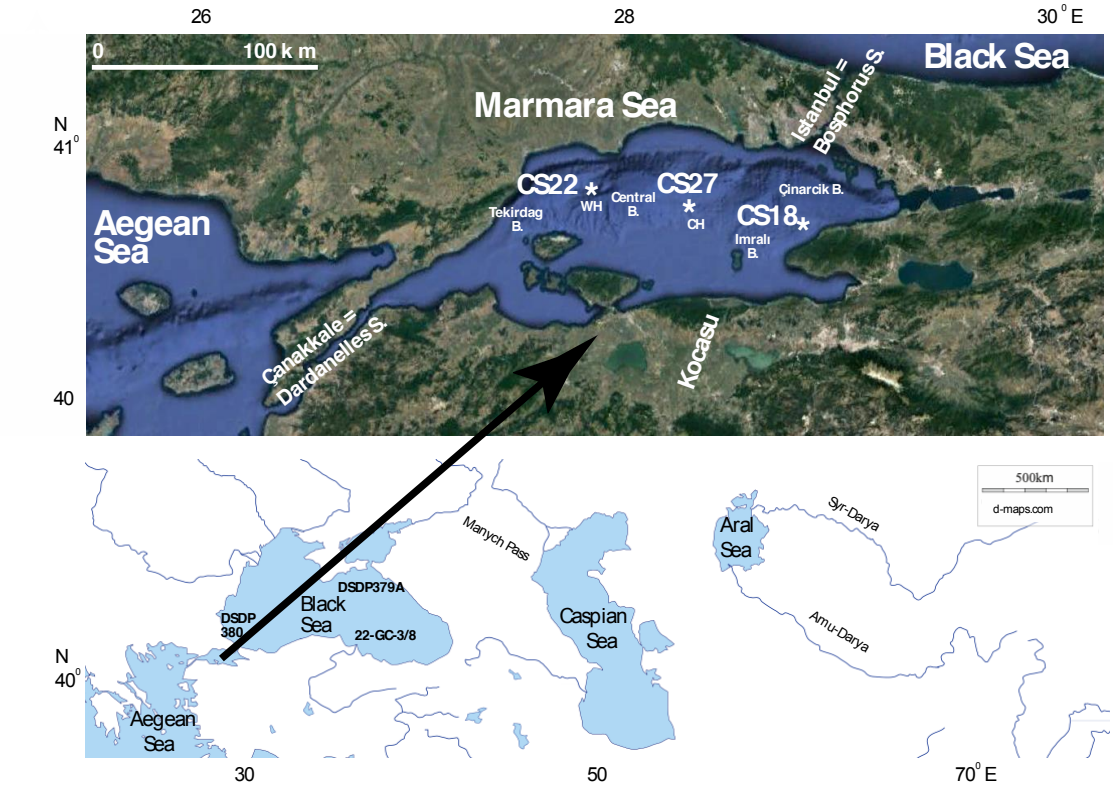

Figure 1: Map of Marmara Sea with core locations (top panel) and map of the seas that were potentially connected at times (lower panel). CH: Central High, WH: Western High, S: Strait, B: Basin.

Owing to a major European research programme, long sediment cores (up to 30 m) were taken in the SoM during the MARSITE cruise in 2014 to address some of those key questions (https://cordis.europa.eu/project/id/308417).

The aim of the current investigation is, by using organic-walled dinoflagellate cyst (herein called dinocyst) analysis (combined to other proxies such as alkenone, diatoms and benthic foraminifera), to establish the conditions at the surface of the water within MIS 5 (130-71 ka ago, Lisiecki and Raymo, 2005) and part of MIS 6 (> 130 ka), and thus to contribute to water-level and surface-water-condition history in the SoM. A sister paper addresses past vegetation, palaeoclimates and chronology on the same samples (Leroy et al., submitted).

2 Regional setting

The SoM (275 km W-E by 80 km N-S) is located at the western end of the North Anatolian Fault where it splits into several strands; as a result, the sea comprises three deep basins (Tekirdag, Central and Çinarcik) separated by two highs: Western High and Central High (Fig. 1). Its deepest location is in the Çınarcık and Central Basins at 1270 m. Rivers are mostly inflowing from the south (Kazancı et al., 2004). The Imralı Basin in the SE SoM is nowadays a flat area of a water depth only around 300-400 m (Yaltırak, 2002). The Kocasu (or River Koca), the main river flowing into the SoM, exits now from the continent, south of the Imralı Island. At lower water levels, it has formed deltas prograding into the Imralı Basin and has largely contributed to fill it; later on, the sediment was fed into the Çınarcık Basin along a now-submerged canyon (Kazancı et al., 2004; Sorlien et al., 2012) (Fig. 1).

The region immediately around the SoM is relatively flat, although mountains up to 2500 m are found in the S and SE and 1000 m in the N.

Water salinity is 22-24 psu at surface and up to 37-39 psu at depth (Beşiktepe et al., 1994; Aydoğdu et al., 2018). The brackish water of the Black Sea (18 psu), being less dense, outflows through the SoM above the deeper denser Mediterranean saline water moving eastwards (Aydoğdu et al., 2018). The pycnocline is at around 25 m water depth. This delicate two-way setting is easily disturbed by water-level changes leading to deep salinity and oxygenation modifications crucial for the survival of aquatic ecosystems. Water temperature fluctuates at most from 4 to 28 ºC annually. It displays a slight warming gradient from the NE to the SW: for example, surface water usually varies from 21 (NE) to 26 (SW) ºC in summer. All year round, bottom water is relatively stable at c.15 ºC (Aydoğdu et al., 2018). The water depth of the Dardanelles (Çanakkale) Sill is nowadays 65 m, and that of the Bosphorus (Istanbul) Sill is 35 m (Çağatay et al., 2009).

The dinocyst assemblages of MIS 6 and 5 have, so far, not been studied in the SoM. However, three dinocyst analyses for these time intervals are available for the Black Sea. In cores DSDP 380 in the SW Black Sea and DSDP Site 379A in the E Black Sea, MIS 5 is covered by a few samples (Ferguson et al., 2018; Hoyle et al., 2021). In the SE Black Sea, a detailed dinocyst diagram of core 22-GC3 includes the period from 129 to 119 ka, with a transition from brackish Pontocaspian to marine conditions at 128 ka (Shumilovskikh et al., 2013) (Fig. 1). More dinocyst records are available for the Late Glacial and Holocene in the SoM (Mudie et al., 2001, 2002, 2004; Londeix et al., 2009) where a change from brackish Pontocaspian to marine conditions was observed at c. 9.5-9 ka. A sapropelic layer, MSAP-1, was identified at 11.5-7 ka ago (Çağatay et al., 2000; Tolun et al., 2002; Vidal et al., 2010). It is worth

mentioning the recent study of dinocyst assemblages on a long core in the Gulf of Corinth, covering the MIS 6 and MIS 5, although further afield, due to the similarity of isolation-connection history of its basin (Fatourou et al., 2023).

Dinoflagellates, a major component of the marine phytoplankton, have a complex life cycle involving a theca that lives in the photic zone and, for about 13 to 16% of the species, an organic-walled cyst is produced in the water column, and settling at the bottom of the sea floor for an obligatory dormancy period (e.g. de Vernal and Marret, 2007; Bravo and Figueroa, 2014; Mudie et al., 2021). Therefore, the distribution of dinocysts in recent sediments has been linked to surface environmental conditions and this relationship has enabled robust quantitative reconstructions of past sea-surface temperature, salinity, productivity and sea-ice cover duration (e.g. de Vernal et al., 2020). A study of 181 surface samples in the Pontocaspian region has clearly highlighted that the dinocyst assemblages reflect surface conditions such as salinity, especially from January to March (Mudie et al., 2017).

3 Previous investigations on cores CS22 and CS18

Calypso cores were taken by the vessel “Pourquoi Pas?” in November 2014. Core MRS-**CS22** (20.42 m long) was obtained close to the top of the Western High at 40,83863 latitude N, 27,79906 longitude E and 551 m water depth (Fig. 1). Core MRS-**CS18** (14.25 m long) was acquired from a slope of the Imralı Basin at 40,66206 latitude N and 28,87958 longitude E by 291 m water depth. The core depths of interest are located below a major seismic reflector, i.e. the red-H1 reflector.

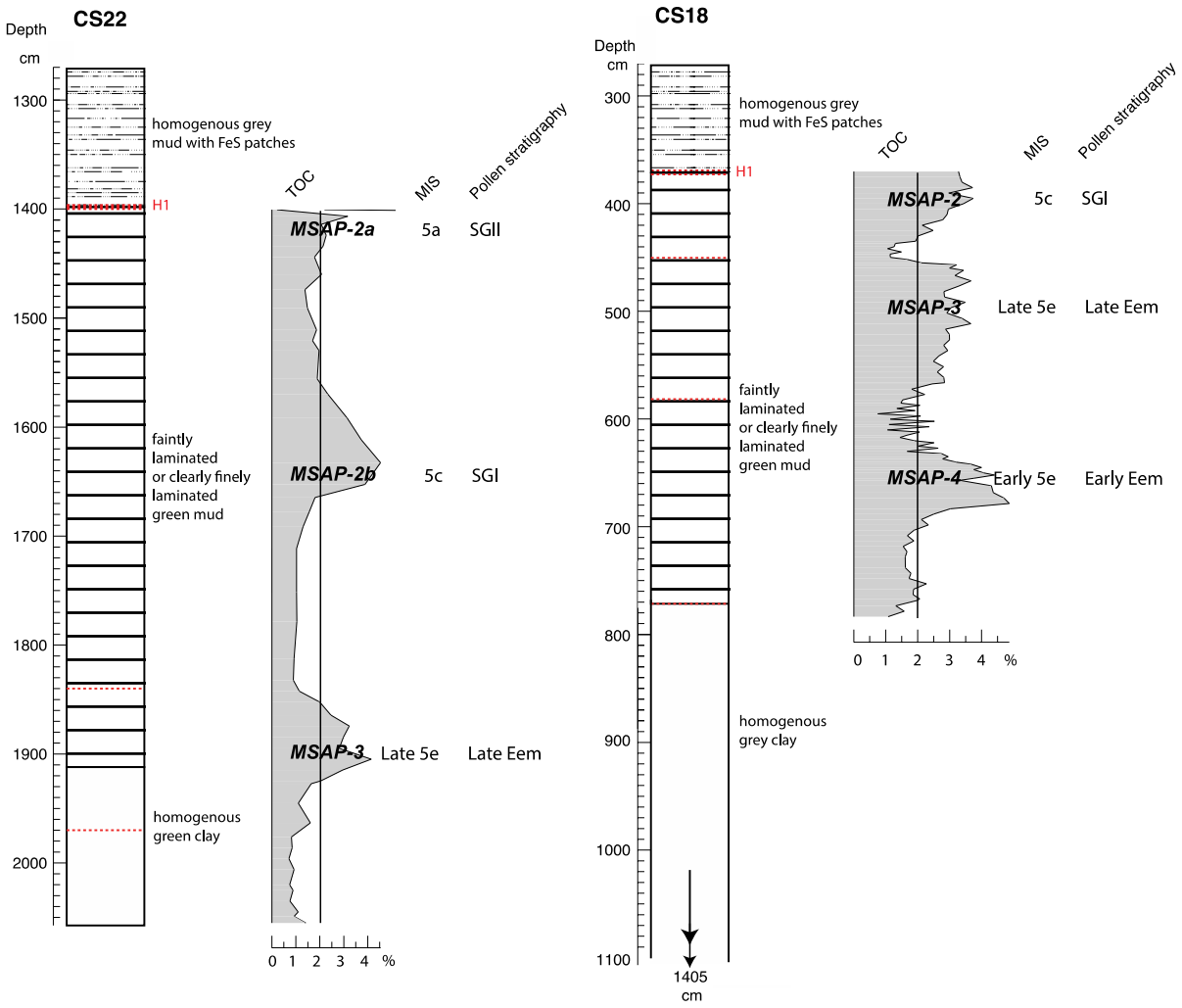

Figure 2: Lithology of cores CS22 and CS18, total organic carbon in percentage (TOC). Vertical line at 2 % delimiting the sapropels. MIS: Marine Isotopic Stages. Me I = Melisey I Stadial, SG I = Saint-Germain I Interstadial, Me II = Melisey II Stadial, SG II = Saint-Germain II Interstadial, Eem = Eemian Interglacial.

Detailed lithological descriptions can be found for cores CS22 and CS18 respectively in Kende (2018) and Çağatay et al. (2019). The sediment is a grey or green clay to silty clay at times clearly finely laminated (Fig. 2). Total Organic Carbon (TOC) values in core CS22 were obtained by using an *Fisons* NA1500 elemental analyser and for core CS18 by the catalytic combustion method using a Shimadzu

TOC analyzer (Kende, 2018; Çağatay et al., 2009; Leroy et al., submitted). In core CS18, foraminifera were counted in the sand size fraction and their abundance were qualitatively recorded. Only rare benthic foraminifera are present in the 770-700 cm interval, but benthic, with some pelagic foraminifera, become abundant in 700-670 cm and 630-580 cm intervals. However, they are absent in the interval 580-430 cm (Çağatay et al., 2019).

Below the red-H1 reflector, the three sapropels (here > 2%) were attributed to MIS 5e, 5c and 5a based on correlation of the µ-XRF Ca with the NGRIP $\delta^{18}O$, the TOC correlation with regional pollen records (outside of the SoM), oxygen isotope records in the Mediterranean and global sea level. These are for core CS18: MSAP-4 at 699-623 cm, MSAP-3 at 568-455 cm and MSAP-2 at 430-370 cm depth (sapropel numbering proposed by Çağatay et al., 2009, 2019). These are for core CS22, MSAP-3 at 1920-1853 cm and MSAP-2 in two parts: MSAP-2b at 1653-1570 cm and to a lesser extent MSAP-2a at 1460-1407 cm (their naming follows what was proposed in Çağatay et al. (2009)). The latter authors have proposed a correlation of the MSAP-4, 3 and 2 to the Mediterranean sapropels S5, S4 and S3. A revision of the two Marmara sequence ages, based on geochemistry and pollen analysis, indicates that for core CS22, MSAP-3 is Late Eemian Interglacial, MSAP-2b is Saint-Germain I Interstadial, and MSAP-2a is Saint-Germain II Interstadial, or approximately MIS late 5e, 5c and 5a (Fig. 2; Leroy et al., submitted). In core CS18, MSAP-4 is early Eemian Interglacial, MSAP-3 is late Eemian and MSAP-2 is Saint-Germain I, or approximately MIS early 5e, late 5e and 5c (Fig. 2; Leroy et al., submitted).

Minor and major hiati are defined and discussed in Leroy et al. (submitted) and shown as red lines on figure 2 and following.

4 Material and Methods

4.1 Dinocyst analysis

Fifty-one sediment samples were treated in core CS22 and 79 in core CS18 mostly below the red-H1 reflector for their palynomorph content. The sampling resolution varied between 10 and 20 cm. After measurement of the sediment volume (between 0.5 and 2.5 ml), one tablet of *Lycopodium clavatum* was added. The sediment was then soaked in tetrasodium pyrophosphate, followed by acid attacks: cold HCl (10% dilution), cold HF (between 40 and 60%) and again cold HCl. Samples were then rinsed with distilled water and sieved on nylon meshes at 125 and 10 µm. The residues were transferred to vials and slides mounted in glycerol. At least 60 dinocysts were counted in each sample, except in core CS22 above 1400 cm, and in core CS18 above 369 cm and below 786.5 cm. Some gritty samples in core CS18 were also centrifuged in Sodium Polytungstate at a density of 2.4. All samples were rich in dinocysts except one at 364 cm depth in core CS18 and one at 2026.7 cm in core CS22. All percentages are calculated based on the sum of all dinocysts, except varia (indeterminate, indeterminable and reworked specimens) and foraminiferal organic linings. Concentration of palynomorphs is calculated in ml of wet sediment. The P/D ratio is the ratio of the concentration of pollen on dinocysts. It reflects the continentality of the sample (McCarthy and Mudie, 1998). The H/A ratio is the ratio of heterotrophic (dependent on nutrients synthesised by other organisms) taxa on autotrophic (whose energy source is the light) ones. Zonation (on 23 and 22 dinocyst taxa respectively in cores CS22 and CS18) was made by CONISS after square-root transformation, available in the psimpoll software (Bennett, 2007), which was also used for plotting dinocyst diagrams. The diversity was calculated using the

Margalef's species richness (Margalef, 1958) and an ordination analysis with non-Metric Multidimensional Scaling (NMDS) (Primer 7; Clarke and Gorley, 2015) allowing distinguishing groups of samples of similar composition.

Identifications were made with the support of the atlas of Mudie et al. (2017), and plates in Marret et al. (2004), Sorrel et al. (2006), Londeix et al. (2009) and Leroy (2010). *Spiniferites cruciformis* specimens were grouped in three different forms (A – standard form, B – pointed apex and C – short and folded processes) as in Marret et al. (2004). *Lingulodinium machaerophorum* ss indicates the sensu stricto form (Leroy et al., 2006; Mertens et al., 2009; Mudie et al., 2017). The "*L. machaerophorum* bulbous" form has short but clearly bulbous (as in Mudie et al. (2017)) and non-clavate processes. *L. machaerophorum* B is described in Leroy et al. (2006), as having short microgranulate processes with a large striated conical base. *Impagidinium* sp. A is a form defined in Londeix et al. (2009). The name *Spiniferites inaequalis* is conservatively used, although some ongoing discussions propose to move the species to the genus *Impagidinium* (Mertens et al., 2018). In the cumulative diagram, the marine taxa are on the left and the brackish Pontocaspian ones on the right. In the middle, are the heterotrophic taxa and the various forms of *Lingulodinium machaerophorum*. Warm-loving dinocysts are defined by the presence of *Operculodinium israelianum, Spiniferites pachydermus, Polysphaeridinium zoharyi, Tuberculodinium vancampoae* and *Spiniferites mirabilis* as they reflect temperatures higher than nowadays (Marret and Zonneveld, 2003; Londeix et al., 2009; Shumilovskikh et al., 2013; de Vernal et al., 2020; Marret et al., 2020). Seasonal contrast in sea-surface temperature (SST) is reflected by *Bitectatodinium tepikiense, Pentapharsodinium dalei* and *Scrippsiella trifida* (Head et al., 2006; Mudie et al., 2017).

Although not dinocysts, coiled organic linings of foraminifera were found and added to this investigation, rather than to the pollen diagram (Leroy et al., submitted), as they usually belong to the marine environments. The inner organic lining is often produced by benthic foraminifera (de Vernal, 2009; Mudie et al., 2021).

4.2 Other proxies in core CS22

Alkenones were measured in sediment samples from core CS22 between 2050 and 1370 cm. After freeze-drying and grinding, samples were extracted using an accelerated solvent extraction system (ASE350, Thermo Scientific). After a clean-up procedure using silica gel column chromatography with a mixture of dichloromethane: hexane (1:1), the total lipid extract was analysed by gas chromatography and flame ionization detection (GC-FID, Trace GC, Thermo Scientific). Identification and purity of alkenones were checked in several samples by gas chromatography coupled to quadrupole mass spectrometry (Trace GC DSQII, Thermo Scientific). GC conditions were similar to those described by Sonzogni et al. (1997). When present, they are considered as marine indicators.

Benthic foraminiferal faunas were quantitatively investigated in the 125 µm fraction from nine samples. At first a qualitative downcore check of foraminiferal content was performed in the coarse fraction at a 1 m sampling resolution, then refined to 20 cm between 2035 and 1915 cm where very rich benthic foraminifera assemblages were found. Two additional samples were investigated at 1632 and 1631 cm. When possible, 300 specimens were counted in sediment aliquots, and identified to the lowest taxonomic level possible, mainly at the species level. To describe major faunal trends, the species Benthic Foraminiferal Number (BFN, expressed as individuals per g or ind.g^{-1}) and frequency data of main species (>1%) were used.

Sediment samples for **diatom and chrysophyte** analyses were collected at 20 cm intervals in each section of core CS22. Smear slides were prepared with a suspension made of known amounts of dry sediment and distilled water. 200 µl of this suspension were spread onto a cover slip, air-dried and mounted on a glass slide using Naphrax mounting medium. Diatom valves were counted along transects and expressed as number of valves per gram of dry sediment. Chrysophycean cysts were also counted; but morphotypes were not identified.

5 Results

Two main types of dinocyst assemblages were observed (Fig. 3 and 4). The first one is largely dominated by *Spiniferites cruciformis* and *Pyxidinopsis psilata*. By comparison to Black, Marmara and Caspian seas Lateglacial-early Holocene assemblages, they are attributed to brackish Pontocaspian conditions, perhaps in the range of ~7-12 psu, thus clearly lower than the surface conditions of the SoM (Bradley et al., 2012; Marret et al., 2004, 2009, 2019). The second assemblage, called here marine, is an assemblage with diverse taxa also with no direct equivalent in the present. It represents salinities probably close to the surface waters of the modern-day Marmara (Balkis et al., 2016).

5.1 Dinocysts in core CS22

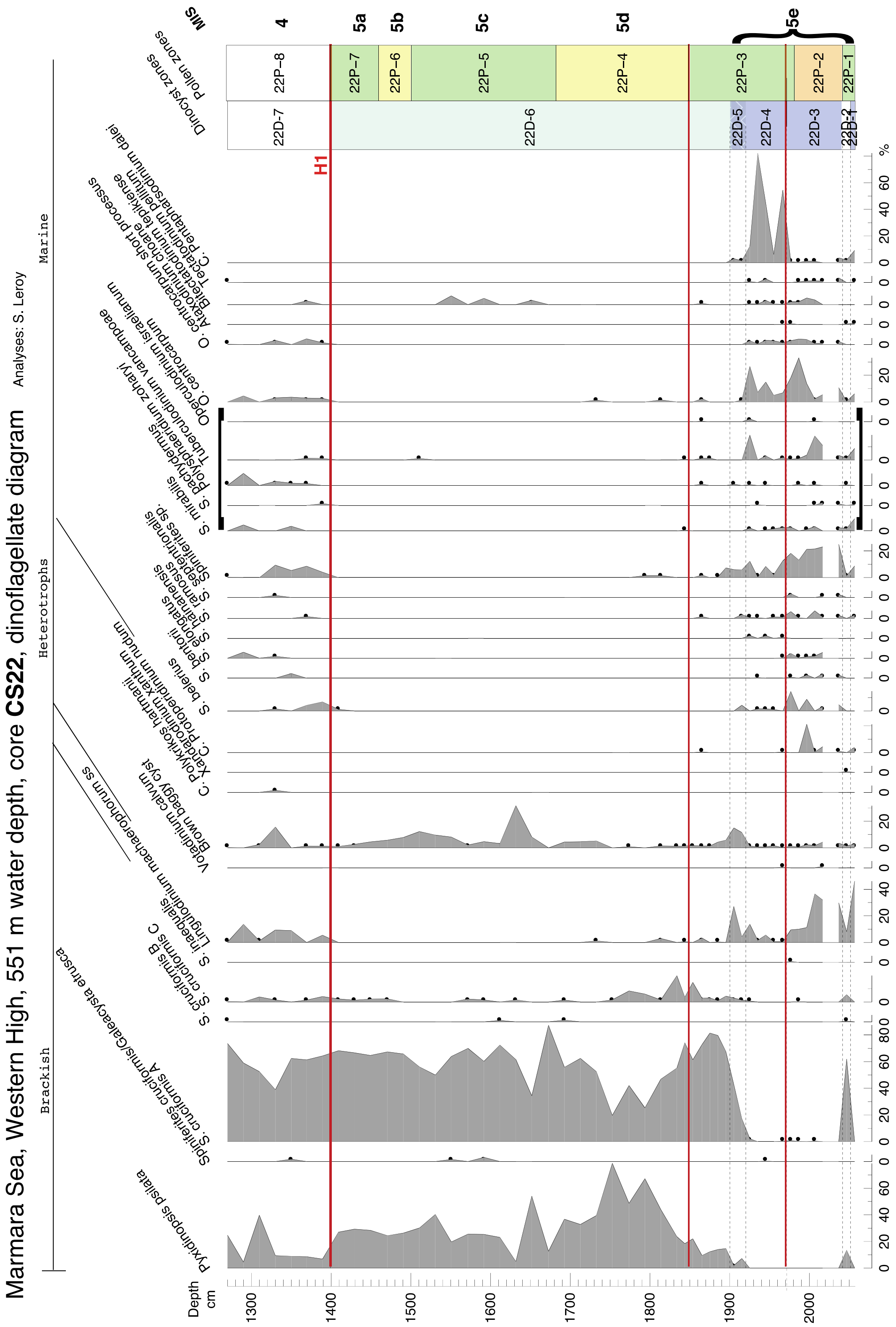
Marmara Sea, Western High, 551 m water depth, core CS22, dinoflagellate diagram
Analyses: S. Leroy
Marine
Heterotrophs
Brackish
MIS
Pollen zones
Dinocyst zones
H1
Depth cm

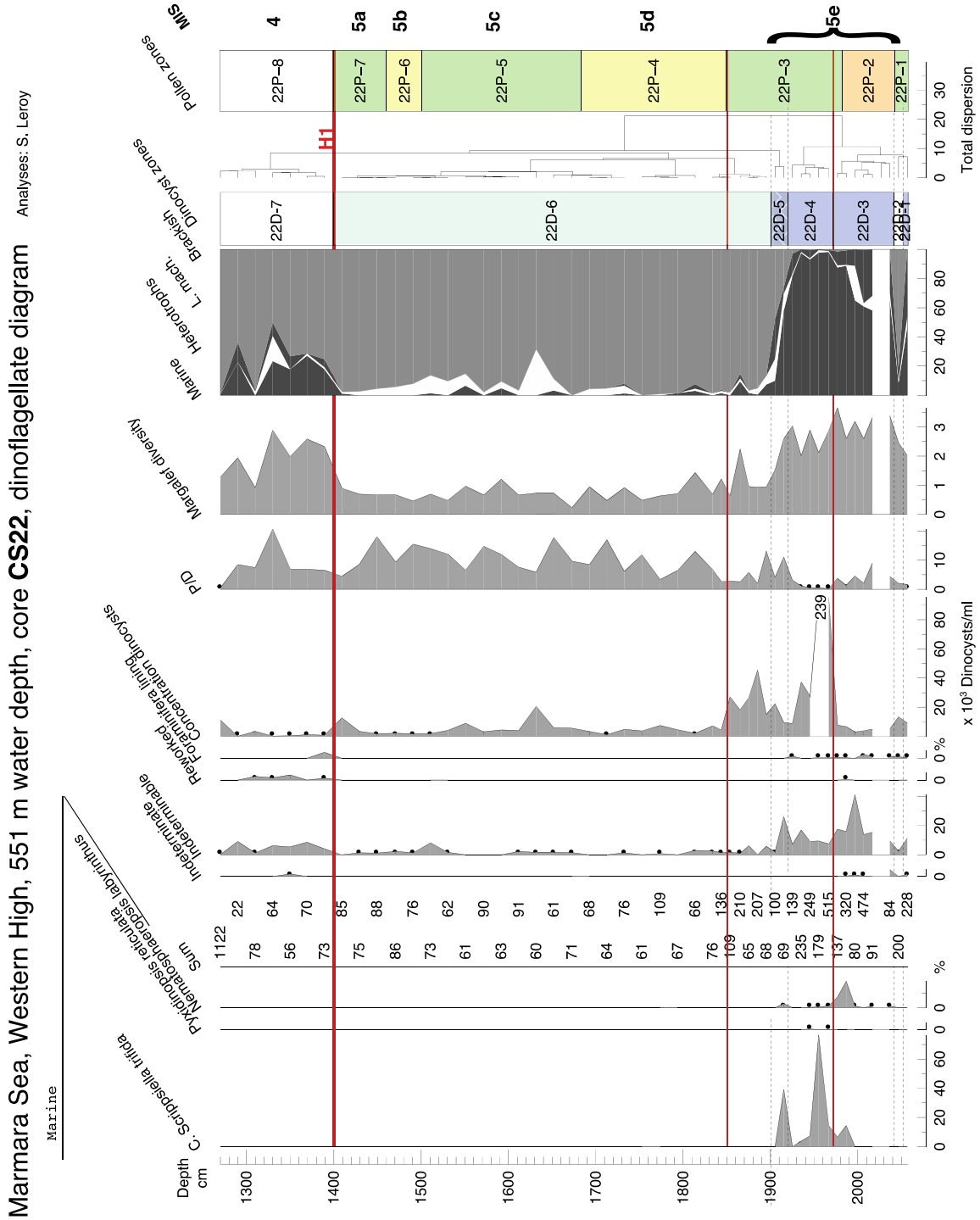

Figure 3 a and b: Percentage dinocyst diagram of core CS22. Black dots for < 5%. Pollen zones to the right with chronological attributions. Horizontal brackets indicate the warm indicators in the marine group.

The dinocyst assemblages show a diversity from 3 to 19 taxa, with notably higher numbers of taxa at the bottom of the core, i.e. below 1920 cm (Fig. 3). Broadly, the record shows a succession of two main assemblages, one mostly dominated by marine taxa, and the following one by brackish Pontocaspian taxa. The main change in the diagram according to the CONISS analysis is by far between zones 22D-4 and 5 at 1920 cm depth (Fig. 3). However, it is not sharp.

Zones 22D-1 and D-2 each consist of one sample (at 2057 and 2047 cm depth). In rapid alternation, the first assemblage is marine with a dominance of *L. machaerophorum* alongside: *Spiniferites sp., S. mirabilis*, cysts of *Pentapharsodinium dalei* and *Tuberculodinium vancampoae*. The second sample has a brackish Pontocaspian assemblage, with the dominance of *Spiniferites cruciformis* A and *Pyxidinopsis psilata* and low occurrence of *L. machaerophorum*. Foraminifera linings are observed in zones D-1 to D-4.

Zone 22D-3 (2042-1972 cm depth): Besides zone 22D-1, *L. machaerophorum* displays its highest values here, declining only in the last third of this zone. The percentages of *Operculodinium centrocarpum* increase progressively to a maximum at the end of this zone. *Spiniferites* sp. also has maximal values. The other taxa, mainly marine, are rather diverse (high Margalef diversity index). A high number of indeterminable cysts occur. The sample at 2027 cm depth is rich in pollen, but hardly contains any dinocysts.

Zone 22D-4 (1972-1920 cm depth): The assemblage is still marine and diverse, but rather different from the previous zone. The spectra are alternatively dominated by

316 cysts of *P. dalei* and cysts of *Scrippsiella trifida*. *L. machaerophorum* is present but in
317 small amounts. The P/D ratio is at its minimum, largely because the concentration in
318 dinocyst is very high, i.e. >230,000 cysts/ml. The number of indeterminable cysts is
319 decreasing but still significant.
320
321 Zone 22D-5 (1920-1900 cm depth): This zone is a period of transition with the
322 percentages of *S. cruciformis* A progressively increasing, and those of *P. psilata*
323 starting a continuous curve, while the marine forms are less diverse (decreasing
324 Margalef diversity index). *L. machaerophorum* makes a brief return. Brown baggy
325 cysts form a bell-shape curve. *Operculodinium centrocarpum* has nearly
326 disappeared. Cysts of *S. trifida* peak in one of the samples.
327
328 Zone 22D-6 (1900-1399 cm depth): This very long (5 m) and rather homogenous
329 (minimal Margalef diversity index) zone is largely dominated by brackish
330 Pontocaspian taxa such as *S. cruciformis* and *P. psilata*. Brown baggy cysts are
331 occasionally more frequent, especially at 1632 cm depth (32%). *Bitectatodinium*
332 *tepikense* is only sub-continuously present in the middle of this zone between 1652
333 and 1551 cm depth. *L. machaerophorum* is occasionally present at the beginning of
334 this zone and soon disappears. All through this zone, the P/D ratio is relatively high.
335 Cyst concentration drops drastically at the very beginning of this zone and remains
336 low for the rest of the sequence.
337
338 Zone 22D-7 (1399-1270 cm depth): The values of *S. cruciformis* remain the same as
339 in the preceding zone, but those of *P. psilata* significantly drop. The assemblage is
340 diverse with many marine forms but with a low occurrence. *L. machaerophorum* is

back with irregular presence between 0.2 and 14 %. Three foraminifera linings (4%) were found at the base of this zone. Concentration is varying, at times below 500 dinocysts/ml. Reworked elements are frequent.

5.2 Dinocysts in core CS18

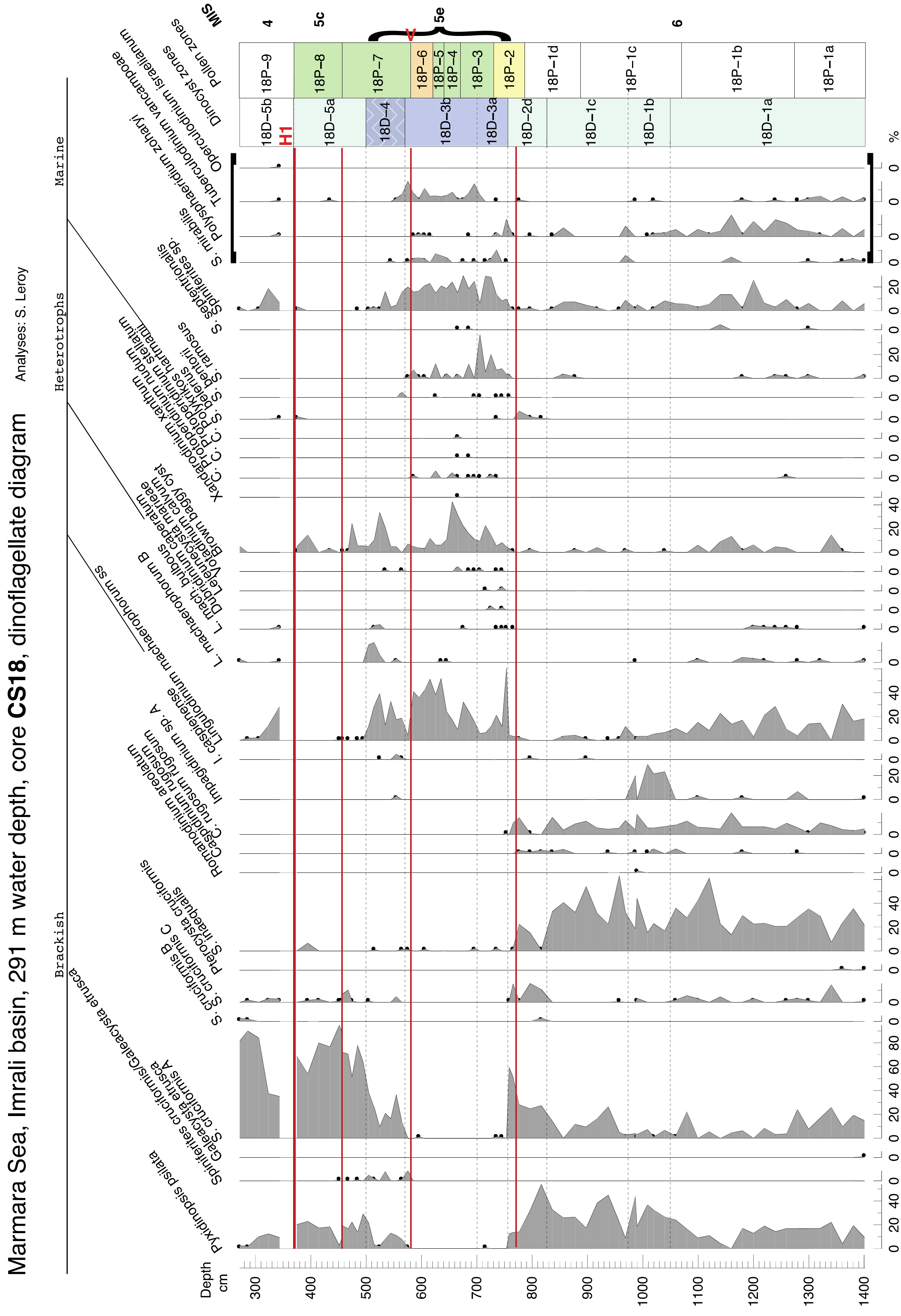

Marmara Sea, Imrali basin, 291 m water depth, core CS18, dinoflagellate diagram
Analyses: S. Leroy
Marine
Heterotrophs
Brackish
MIS
Pollen zones
Dinocyst zones
4
5c
5e
6
H1
18P-9
18P-8
18P-7
18P-6
18P-5
18P-4
18P-3
18P-2
18P-1d
18P-1c
18P-1b
18P-1a
18D-5b
18D-5a
18D-4
18D-3b
18D-3a
18D-2d
18D-1c
18D-1b
18D-1a
Operculodinium israelianum
Operculodinium vancampoae
Tuberculodinium vancampoae
Polysphaeridium zoharyi
S. mirabilis
Spiniferites sp.
S. septentrionalis
S. ramosus
S. bentorii
S. hartmanii
S. belerius
C. stellatum
C. nudum
C. polykrikos
Protoperidinium
Xanthum
Xandarodinium
Brigantedinium
Votadinium calvum
Lejeunecysta marieae
Dubridinium caperatum
L. machaerophorum B
L. machaerophorum ss
Lingulodinium machaerophorum
I. caspienense
Impagidinium sp. A
C. rugosum rugosum
Caspidinium rugosum
Romanodinium areolatum
S. cruciformis
Pterocysta cruciformis
S. inaequalis
S. cruciformis B C
Spiniferites cruciformis/Galeacysta etrusca
Galeacysta etrusca
S. cruciformis A
Pyxidinopsis psilata
Depth cm
300
400
500
600
700
800
900
1000
1100
1200
1300
1400
%

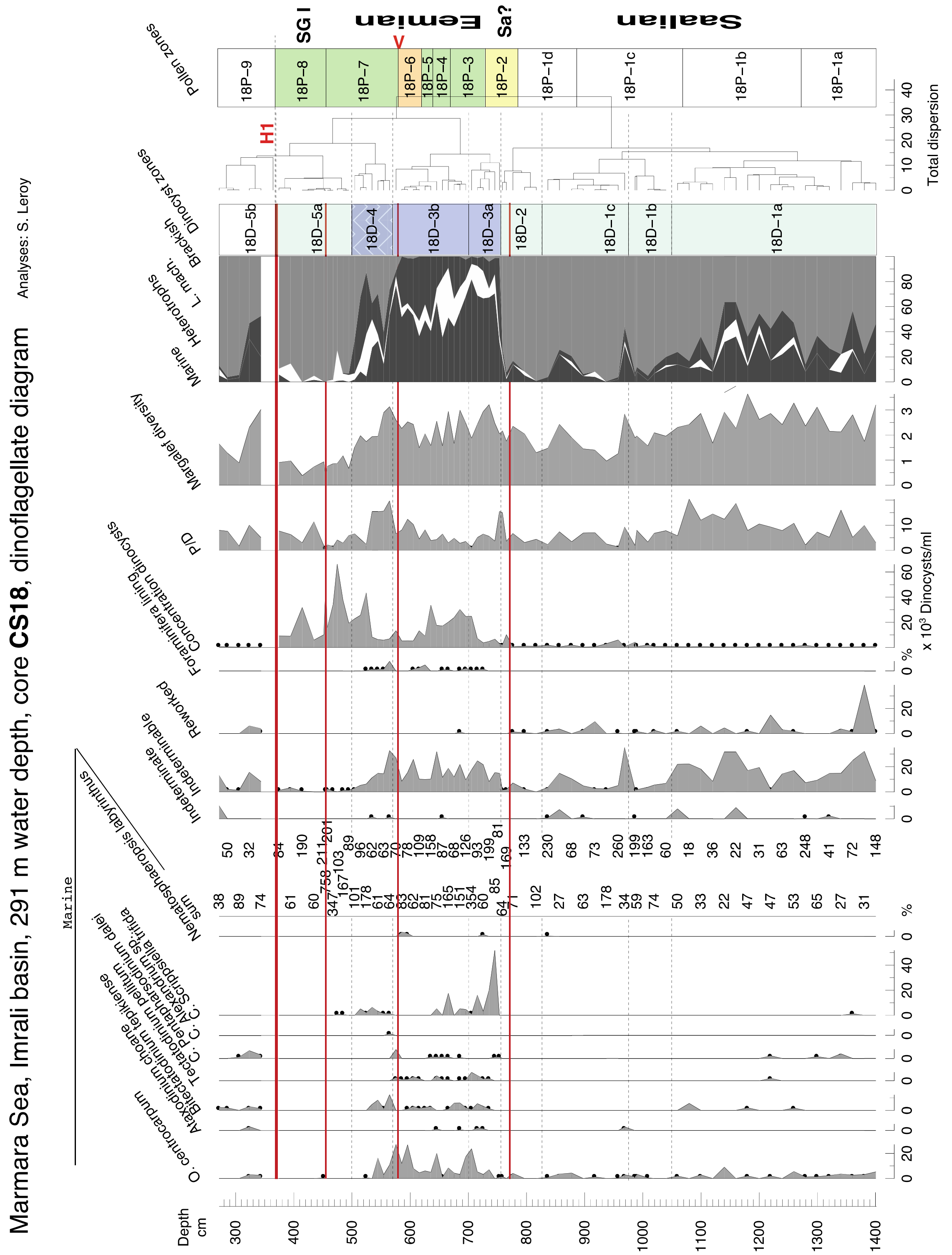

Figure 4 a and b: Percentage dinocyst diagram of core CS18. Black dots for < 5%. Pollen zones to the right with chronological attributions. Horizontal brackets indicate the warm indicators in the marine group.

The dinocyst assemblages show a diversity from 3 to 17 taxa, with notably higher numbers of taxa below 1180 cm, and at 735 and 565 cm (Fig. 4). Broadly, the record shows the succession of three main assemblages, one mostly dominated by marine taxa in the middle, with below and above it two brackish Pontocaspian assemblages of two different types. The two main changes in this diagram are at 756 and 570 cm depth (Fig. 4).

Zone 18D-1, 1400.5 – 826.5 cm depth: This is a very long zone of nearly 6 m. It is dominated by brackish Pontocaspian taxa such as *P. psilata*, *S. cruciformis* A, *S. inaequalis* and *Caspidinium rugosum rugosum,* with a significant occurrence of *L. machaerophorum ss*. In general, concentrations are relatively low, mostly below 1000 cysts/ml. Reworked cysts are frequent. This zone has been subdivided into three subzones, with subdivisions as followed. Subzone 18D-1a (1400.5-1049.5 cm) is dominated by *S. inaequalis*. *L. machaerophorum ss, P. psilata* and *S. cruciformis* A are abundant. A range of marine and brackish Pontocaspian taxa occur side by side. Indeterminable dinocysts are abundant. A large peak of reworked cysts occurs at 1381 cm depth. The P/D ratio remains high all through this zone, with maximal values towards the end, i.e. a maximum of up to above 20. Concentrations are very low, often lower than 500 cysts per ml. Subzone 18D-1b (1049.5-977 cm): This zone is characterised by a bell-shaped curve of *Impagidinium* sp. A. *S. inaequalis* is still abundant. *P. psilata* displays increasing values across this zone. In subzone 18D-1c (977-826.5 cm)*, P. psilata* reaches maximal values, i.e. 54%. The percentages of *S. inaequalis* are still high. Less diverse marine forms are observed.

Zone 18D-2, 826.5-756 cm depth: This zone is characterised by many changes. *P. psilata* decreases and *S. cruciformis* A increases up to a brief maximum of 59%. *S. cruciformis* C is very abundant. A small bell-shaped curve of *S. belerius* occurs. *S. inaequalis* values drop. Very few marine taxa subsist. Concentrations are slightly increasing. This zone represents a transition that is truncated by a hiatus, recognised as one the strongest statistical changes according to CONISS.

Zone 18D-3, 756-570 cm depth, is a totally different zone, with *L. machaerophorum* (up to 52%) and *Spiniferites* sp. (up to 30%) widely dominant. Brown baggy cysts are very abundant in this zone and the following one, i.e. up to 30%. Many marine taxa are present. *S. ramosus*, *O. centrocarpum* and *Tuberculodinium vancampoae* are well represented. Concentrations are high, often around 10,000-20,000 dinocysts/ml. A split into subzones 3a and 3b at 700.5 cm depth is based on a maximum of *S. ramosus,* very large peak of cysts of *S. trifida* (52%), medium-high concentration and maximum percentage of marine taxa in subzone 3a; whilst in subzone 3b high *T. vancampoae* and high concentration occur. This zone ends with the second strongest diagram change (as calculated by CONISS). Foraminiferal linings are only present in this zone and in the following zone.

Zone 18D-4, 570–499.5 cm depth, appears as a transition, with mixed marine and brackish Pontocaspian assemblages. *P. psilata* and *S. cruciformis,* quasi absent in zone 18D-3, reappear. *L. machaerophorum* (with a peak of other forms of *L. machaerophorum* towards the end of this zone) and brown baggy cysts are still

abundant. Marine taxa remain present, but their values decrease. Concentrations, after moderate values, become high again. P/D is maximal, i.e. up to just below 20.

Zone 18D-5, 499.5-271.5 cm, is split in two by the seismic red-H1 reflector; moreover, a barren sample occurs a few cm above this stratigraphic hiatus. In subzone 18D-5a, 499.5-369 cm depth, *S. cruciformis* A very largely dominates with percentages up to 95%. Besides *P. psilata* and brown baggy cysts, hardly any other taxa are present. It is noteworthy that *L. machaerophorum* has only rare occurrences in this subzone, and only at its base. This is a very low diversity subzone (minimum in the Margalef index). Concentrations, after being very high, become high, i.e. 66,000 to 10,000 dinocysts/ml. Subzone 18D-5b, 369-271.5 cm depth: The assemblages are similar to subzone 18D-5a (dominance of brackish Pontocaspian taxa), but brown baggy cysts have quasi disappeared and are replaced by *L. machaerophorum* that have re-appeared. A moderate range of marine taxa is present. Concentrations are very low as in subzones 18D-1a. Reworked elements are common in the lower half of this subzone, just above the barren sample.

5.3 Other proxies in core CS22

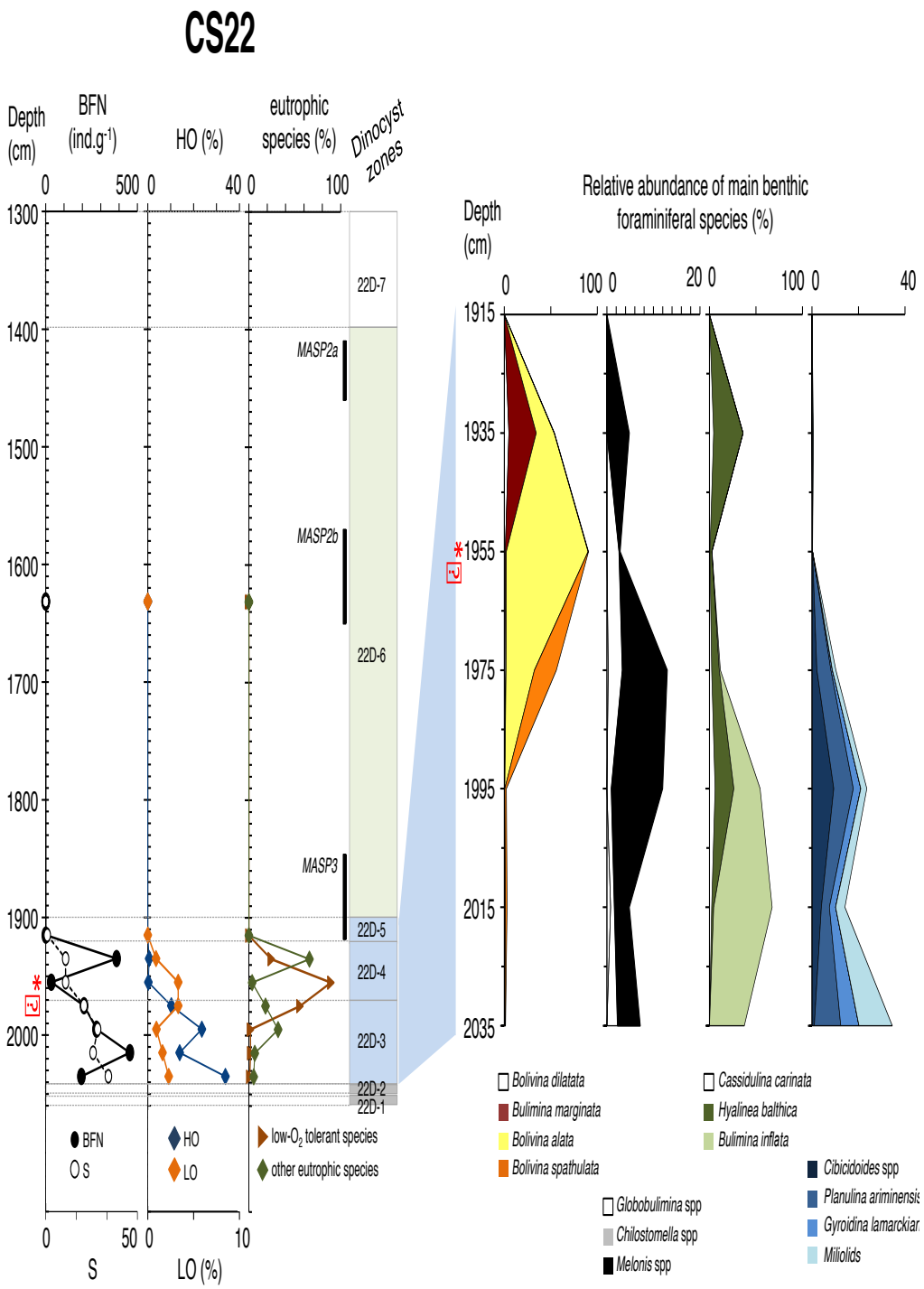

Figure 5: Benthic foraminiferal record of core CS22 with dinozones and Marmara sapropels (MSAP). Right panel: relative abundance of main species (>3%) between 2035 and 1915 cm depth. Left panel: Benthic Foraminiferal Number, BFN (ind.g^{-1}),

species richness S, relative abundance of ecological groups of species. HO = species adapted to high-oxygen level, LO = low-oxygen indicators, eutrophic species = species adapted to high organic carbon fluxes. For further explanation on ecological assignment of species, the reader is referred to the discussion and Table SI2.

Quantitative investigation of benthic foraminiferal assemblages relies on the recovery of a well-preserved, abundant (164 to 361 specimens) and diverse (>60 species overall) faunal content between 2035 and 1915 cm depth (Table SI1). Apart from a few individuals (< 10) belonging to neritic taxa (e.g. *Ammonia*, *Discorbinella*, *Elphidium*), assumed to be post-depositional, foraminiferal assemblages overwhelmingly consist of species from marginal to bathyal environments. The BFN ranges from 30 to 459 ind.g^{-1}, with lowest values recorded at 1955 cm. Dominant species (>5%) belong to *Bolivina* spp, *Bulimina* spp, *Cassidulina carinata*, *Cibicidoides* spp, *Hyalinea balthica* and *Melonis* spp and indicate fully marine conditions at the seafloor at the base of the core. The foraminiferal record, though short, exhibits a marked species shift between 1995 and 1975 cm (Fig. 5). From 2035 to 1995 cm, species number is highest, ranging from 31 to 41. Faunas are strongly dominated by *Bulimina inflata* (28-63%), together with various associated species including *Cibicidoides* spp (1-9%), *Gyroidina lamarckiana* (3-8%), *Planulina ariminensis* (3-11%) and miliolids (3-14%). Minor species (<3%) include *Bulimina aculeata*, *Uvigerina mediterranea* and *U. peregrina*. From 1975 up to 1935 cm, most of the afore-mentioned species disappear from the record. Dominant species consist mainly in *Bolivina alata*, *B. spathulata* and *Bulimina marginata*, which collectively account for 49 to 90% of the assemblage. Concomitant to this faunal shift, species

number drops from 25 to 13 (Fig. 5). By contrast, several other species such as *Cassidulina carinata*, *Hyalinea balthica*, *Melonis affinis* and *M. pompiloides* exhibit no clear upcore trend. Present along the whole record, these species show punctual increases, as especially marked for *H. balthica* at 1995 (32%) and 1935 (20%) cm. Sample at 1915 cm is considered barren of benthic foraminifera as fourteen reworked individuals only were found. Samples at 1632 and 1630 cm were devoid of any foraminifera.

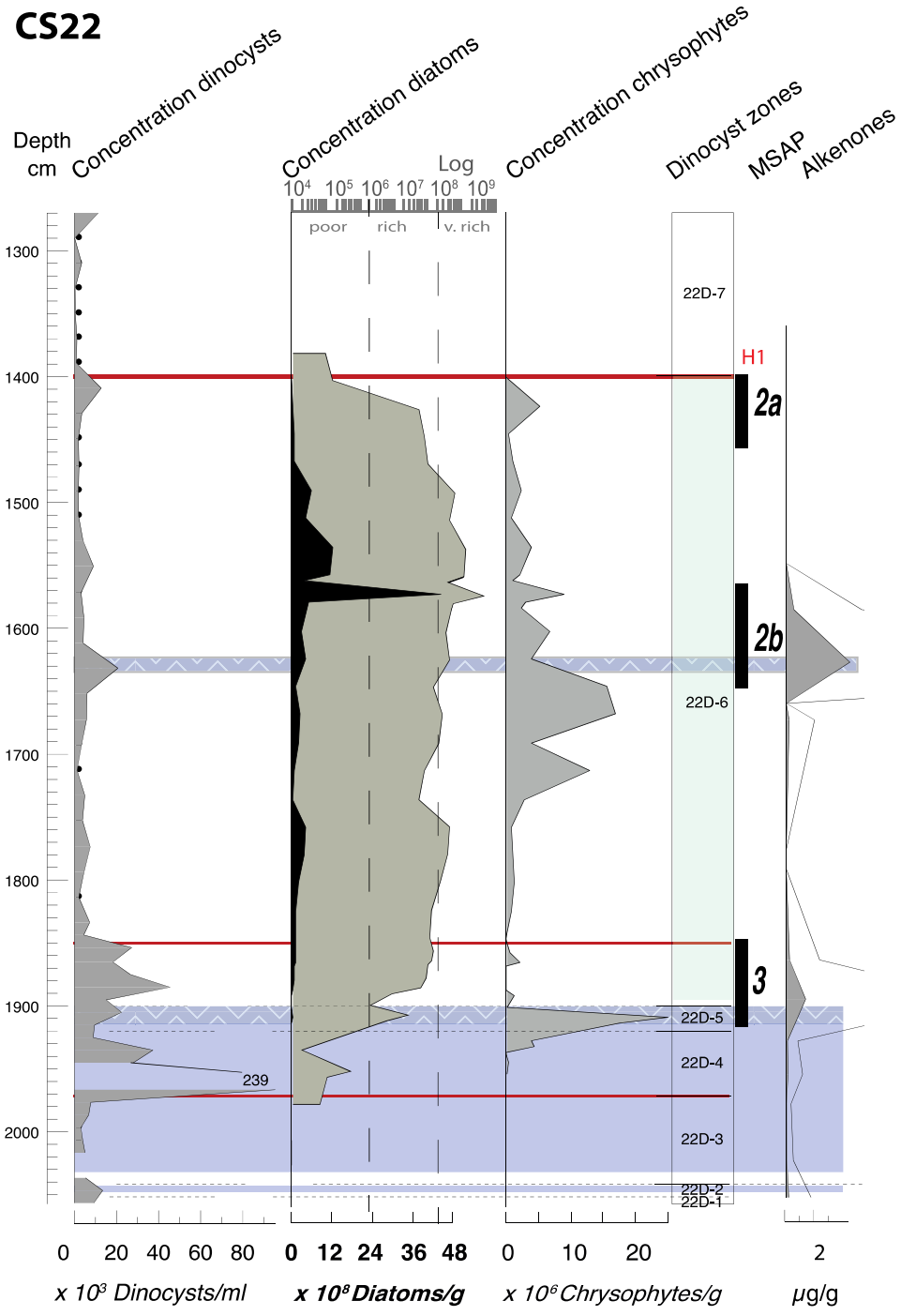

453

454 **Figure 6:** Palaeoproductivity: concentrations of dinocysts, diatoms (in decimal and

455 log scales) and chrysophytes, with dinozones, alkenones and Marmara sapropels

456 (MSAP) in core CS22. The second marine phase at 1633-1632 cm depth is indicated

457 by a box with a blue zigzag highlight.

458

Diatom preservation is becoming better from bottom to the red-H1 reflector. Hardly any diatoms were found below 1915 cm (Fig. 6). Then only some occurrences are noted between 1915 and 1866 cm. From 1854 cm upwards and until 1470 m, the diatom concentrations are high to very high. Diatom concentrations are the highest between 1591 and 1491 cm depth. Chrysophycean cysts are abundant when diatom concentrations decrease. The diatom assemblages are composed of a mixture of fresh and brackish-water species. Dominant *Stephanodiscus* species (*S. minutulus, S. parvus, S. medius, S. neoastrea, S. hantzschii*) occurred with numerous fragments of *Entomoneis calixasini*, a fossil species so far only found in core sediments of the SoM (Pailles et al., 2014). The first occurrence of *E. calixasini* in core CS22 is recorded at 1834 cm depth. Spores of a marine planktonic diatom, *Chaetoceros,* are observed from 1850 to 1830 cm.

The values of alkenones are usually below detection limit, except at 2050-1865 cm and 1633-1592 cm, reaching respective maxima of 1.3 µg/g at 1896 cm and 4.4 µg/g at 1633 cm depth (Fig. 6).

6 Interpretation and discussion

6.1 Core CS22: taphonomy, surface water condition and chronology

6.1.1 Taphonomy

Below the sapropel

At 2027 cm in zone 22D-3, the sample is unexpectedly barren in dinocysts. It is one of the samples of zone 22P-2 with abundant *Pinus* pollen (76%) (Leroy et al., submitted). The lithology shows a bioturbated sediment. Sediment disturbance may also contribute to explain the rapidly changing spectra in the short zones 22-D1 and

D2. The sharp zone limit at 1920 cm (between zones 22D-4 and 5) corresponds to a very thin silt layer and a change from bioturbated to unbioturbated sediment, that is the start of the sapropel attributed to MSAP-3 (1920-1853 cm).

In the sapropel and above

Dinocysts (as well as pollen) are well preserved and their concentrations are maximal as observed in other sapropels (Cheddadi and Rossignol, 1995; Kotthoff et al., 2008) (Fig. 6).

Impact of red-H1 seismic reflector

With the red-H1 reflector (a hiatus), a long-term change in taphonomy is initiated in the SoM. It is seen in the reworking of older marine layers and of soils. Firstly, some foraminifera (linings) are brought in the sediment. Secondly, the non-pollen palynomorphs *Glomus* (a fungal spore) is present, due to inwash of soil erosion products (Leroy et al., submitted). This reflects a turning point in the aquatic conditions of the SoM.

6.1.2 Sea-surface and bottom conditions

The depths of 2042-1920 cm (dinocyst zones 22D-3 and 4) are fully marine as clearly seen not only in the dinocyst assemblages but also in the alkenone values and the benthic foraminiferal content (Fig. 3, 5 and 7).

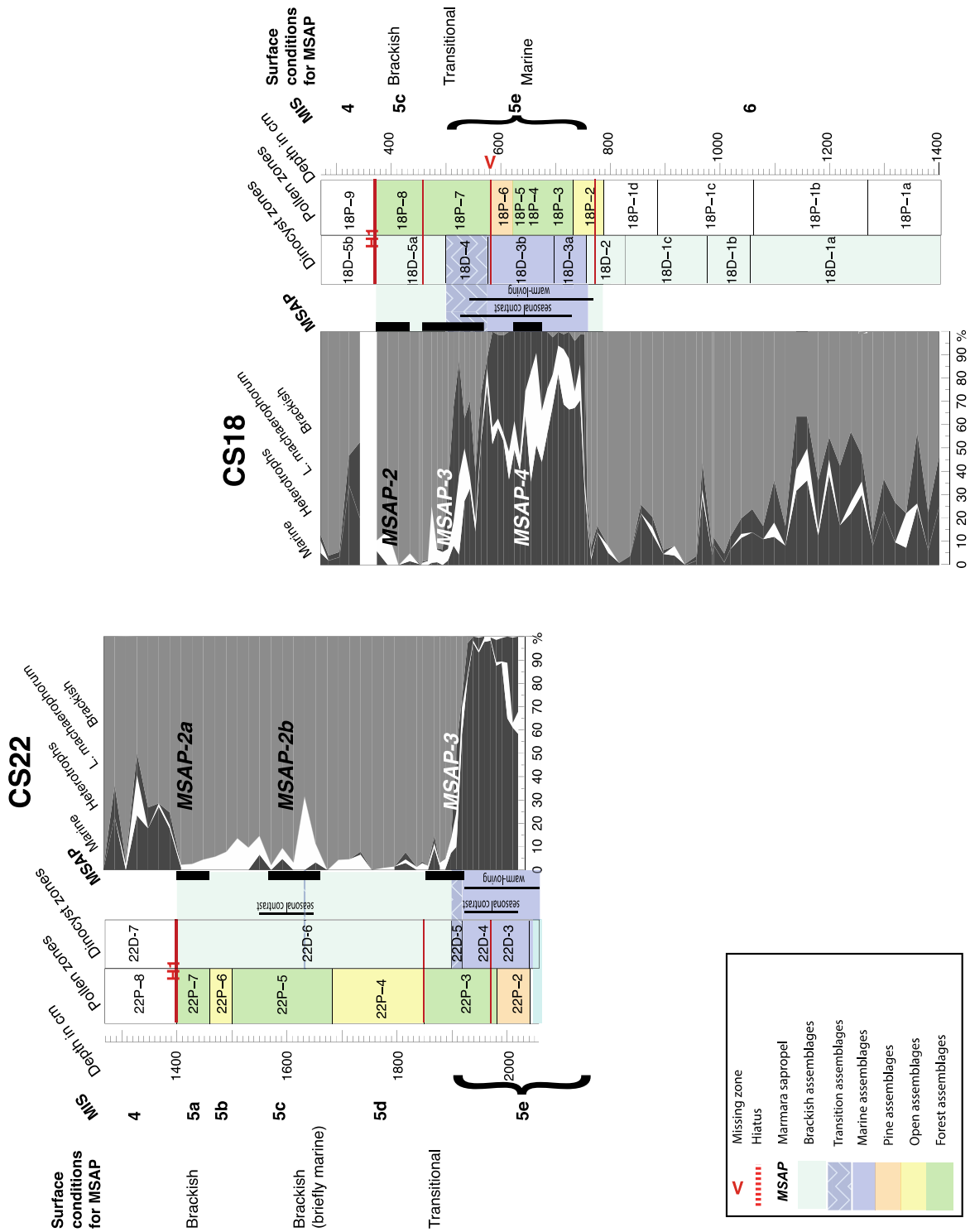

Figure 7: The cumulative diagrams sorting dinocyst groups/taxa by salinity. The four groups are the marine ones (black) to the left, the brackish Pontocaspian dinocysts (grey) to the right), and in the middle the heterotrophic cysts (white) and the *Lingulodinium machaerophorum* forms (black). Dinocyst zones: blue highlight for marine, light blue for brackish Pontocaspian. The distribution of warm-loving and

seasonal contrast indicators as vertical black lines. Pollen zones: green highlight for high arboreal taxa (minus *Pinus*) zones and yellow for low arboreal taxa % and high *Pinus* % zones. Horizontal bold V for pollen and dinocyst zones absent in core CS18.

Five indicators of warm sea-surface temperature (SST) are recorded: *O. israelianum, S. pachydermus, P. zoharyi, T. vancampoae* and *S. mirabilis* (Fig. 3 and 7). They are especially abundant in zone 22-D3. Their occurrence suggests temperatures higher than nowadays. *B. tepikiense,* occurring in zones 22-D3 and 4, reflects marine conditions with seasonal amplitudes of SST. Thus conditions recorded in zone 22-D3 suggest a warm climate with seasonal contrast.

In zone 22D-4 at 1955 cm, high values of cysts of *P. dalei* and *S. trifida* suggest an increase in temperature seasonality and lower salinity (e.g. Head et al., 2006; Mudie et al., 2017). In contrast, very high concentrations point at surface waters rich in nutrients and possibly bottom waters with low oxygen (Mudie et al., 2017). This may be due to alternating deep-water upwelling - when the heavy saline marine waters penetrate the bottom of the basin from the Aegean Sea - and stratification. This occurs below the horizon with high TOC (sapropel MSAP-3 at 1920-1853 cm depth and bottom anoxia, Fig. 2).

To tackle environmental changes at the seafloor, the approach of Cornuault et al. (2016, and references therein) was followed and foraminiferal species were gathered into three functional groups assumed to be representative of contrasted oxygen and trophic conditions at the seafloor: (1) species adapted to high oxygen conditions (HO), (2) low-oxygen indicators (LO), and (3) species adapted to eutrophic conditions (Fig. 5). Ecological assignment is given in Table SI2. The major

faunal shift observed at 1995 -1955 cm suggests contrasted oxygen conditions between zones 22D-3 and 22D-4, possibly related to the establishment of eutrophic conditions. In zone 22D-3, benthic foraminiferal assemblages are ecologically diverse and consist of a mix of epibenthic and various endobenthic species. This sequence and the high abundance of HO species suggest a mesotrophic environment where well-oxygenated conditions prevailed at the seafloor. By contrast, HO indicators disappearance in zone 22D-4 together with high abundance of species adapted to high organic fluxes points to reduced oxygen level during this phase. Assemblages from this zone are successively dominated by species adapted to contrasted oxygen conditions, suggesting variable oxygenation level during zone 22D-4. In particular, the BFN decrease, high dominance of eutrophic species tolerant to low-oxygenation and slight increase of LO species suggest dysoxic conditions at the beginning of this period at 1935 cm, high dominance of species adapted to moderate oxygen depletion strongly suggest environmental changes recorded at the seafloor directly are related to eutrophication rather than ventilation changes. Overall the foraminiferal assemblages confirm the presence of oxygen at the bottom of the sea in zones 22D-3 and 22D-4.

In the dinocyst diagram (Fig. 3), the P/D ratio, informing on the intensity of terrestrial influence on the aquatic realm, is extremely low in zone 22-D4. It is low in general below the hiatus at 1845-1842 cm depth. It is relatively high above it with values frequently higher than 10. It is therefore suggested that the water level was the highest in zone 22-D4 (1972-1920 cm). This is just before the high TOC values linked to the MSAP-3 sapropel.

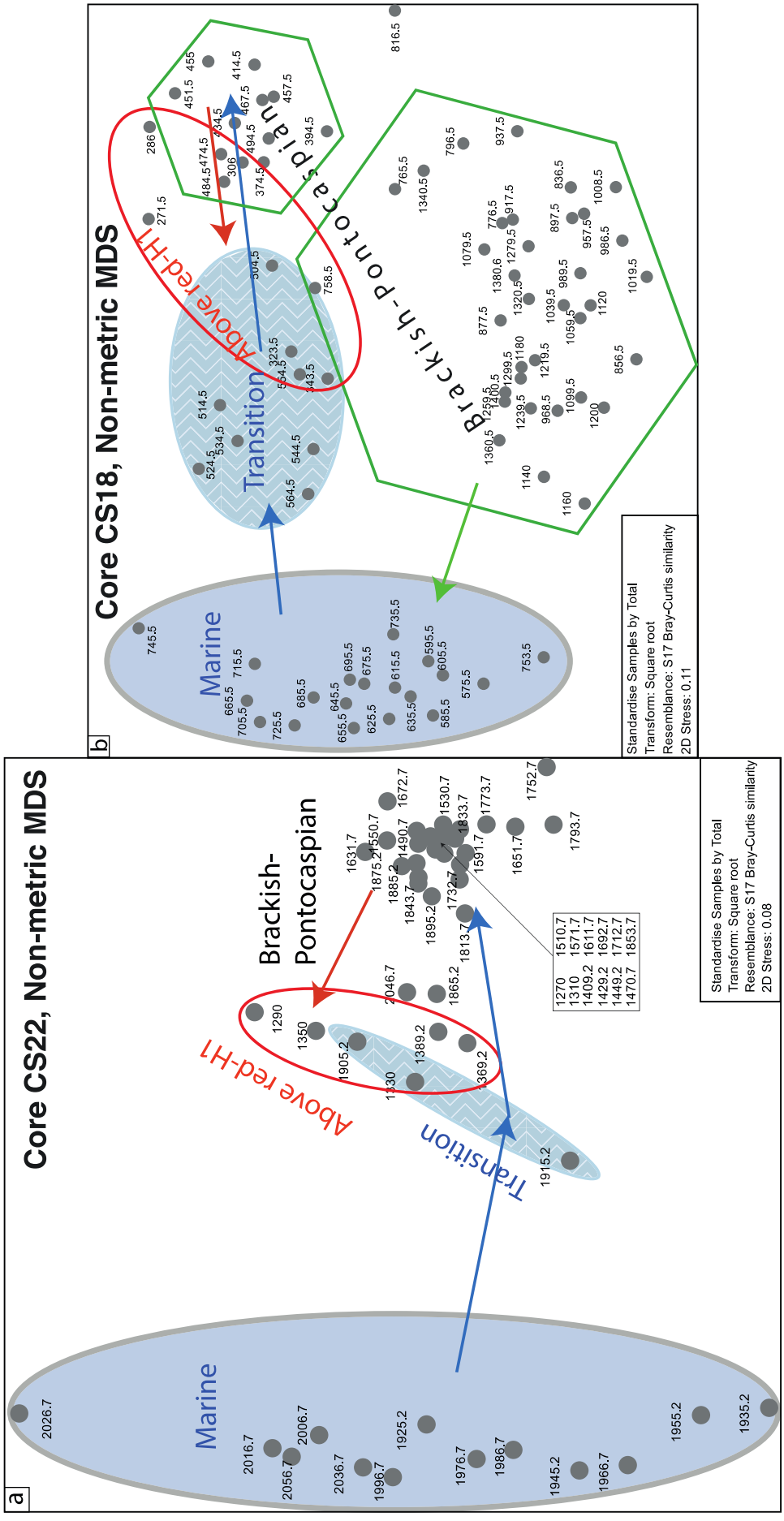
a
Core CS22, Non-metric MDS
Marine
Brackish-Pontocaspian
Above red-H1
Transition
Standardise Samples by Total
Transform: Square root
Resemblance: S17 Bray-Curtis similarity
2D Stress: 0.08
b
Core CS18, Non-metric MDS
Marine
Transition
Above red-H1
Brackish-Pontocaspian
Standardise Samples by Total
Transform: Square root
Resemblance: S17 Bray-Curtis similarity
2D Stress: 0.11

559 **Figure 8**: Results of the NMDS analysis on dinocyst percentages from cores CS22
560 (a) and CS18 (b). Depth in cm.
561
562 Zone 22D-5 (1920-1900 cm) is a transition zone towards brackish
563 Pontocaspian conditions (also seen in the NMDS results in figure 8). The
564 disappearance of foraminiferal shells at 1915 cm is attributed to bottom anoxic
565 conditions in the subsequent MSAP-3 (1920-1853 cm).
566 Then zone 22D-6 (1900-1399 cm) is clearly brackish Pontocaspian, as seen
567 in dinocysts and in the diatom species that indicate fresh to brackish conditions.
568 Interestingly, marine *Chaetoceros* spores occur at 1850-1830 cm. The highest
569 concentrations of Chrysophycean cysts indicating fresher / more oligotrophic
570 conditions occurred between 1680 and 1611 cm depth when diatom concentration
571 decreases. Later, between 1591 and 1491 cm, the highest diatom concentrations
572 recorded suggest increased seasonal productivity.

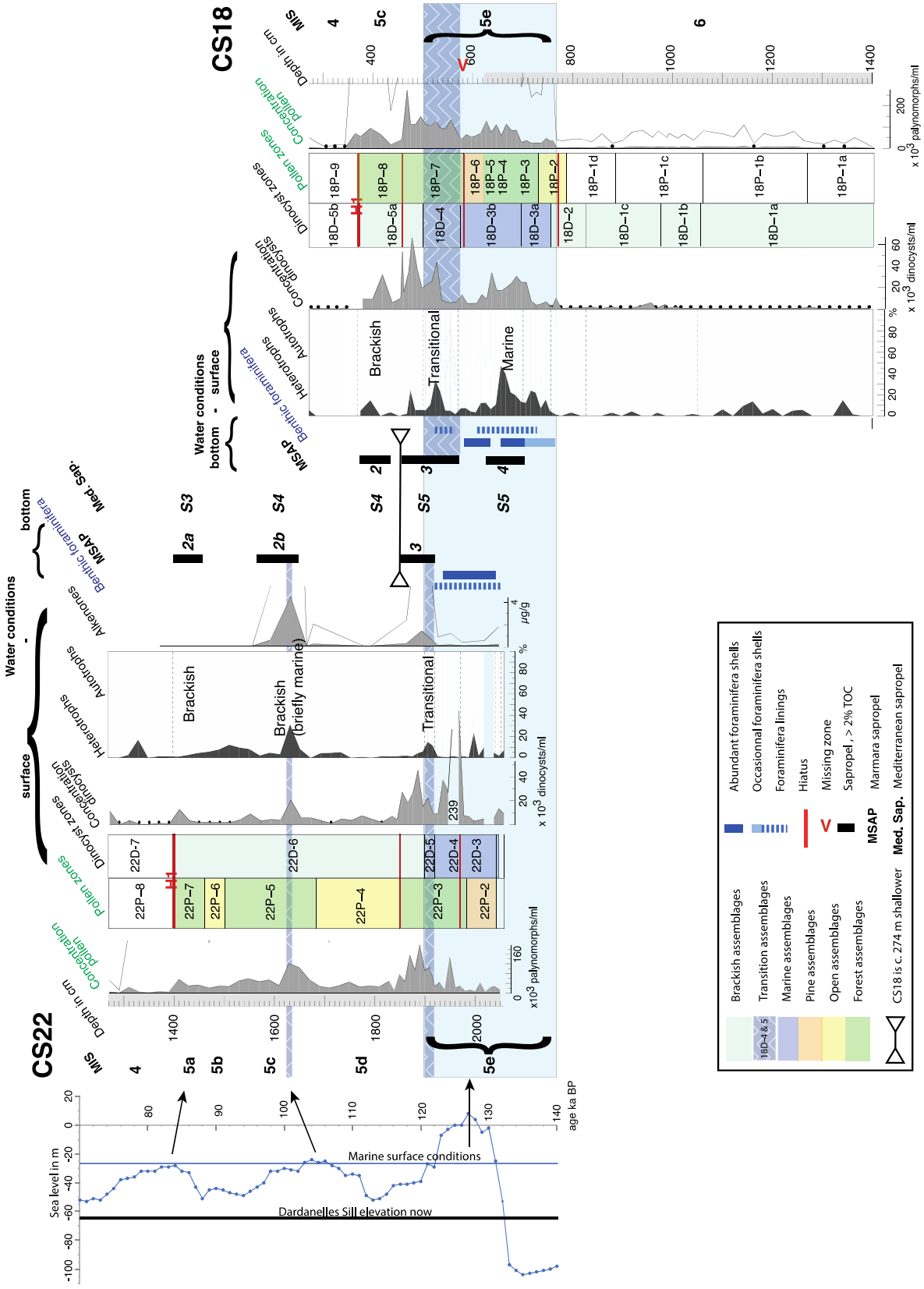

573

574 **Figure 9**: Water conditions. At the surface, dinocyst concentration and the ratio

575 heterotrophic and autotrophic dinocysts (H/A). In the middle for core CS22, also the

alkenones. For the bottom: Marmara sapropels (MSAP, >2% TOC), benthic foraminifera shells and benthic foraminifera organic lining. The top of the marine horizon in core CS18 (hiatus between zones 18P-7 and 8) is c. 274 m deeper than that in core CS22 (hiatus between zones 22P-3 and 4). Horizontal bold V for pollen and dinocyst zones absent in core CS18. For linking with the sister paper on pollen (Leroy et al., submitted), pollen zones and pollen concentrations are also shown. By combining the two light grey vertical boxes, the most complete record is obtained. Sea-level curve from Rohling et al. (2021) with the position of the Dardanelles Sill elevation now (-65 m) and the sea-level threshold where transition from brackish to marine conditions occurred.

However this long 22D-6 zone is not homogenous. At 1632 cm, a peak of heterotrophic dinocyst is observed. It seems to correspond to the second peak in alkenones, indicating marine influence, at 1633 cm (Fig. 9). According to pollen analysis, it is in an interstadial (Saint-Germain I). Thus, a brief marine incursion is probable. It is located at the beginning of sapropel MSAP-2b at 1653-1570 cm.

Zone 22D-7 (above 1399 cm, above the red-H1 seismic reflector) suffers from taphonomical problems (Leroy et al., submitted). Nevertheless, it is mainly brackish-Pontocaspian, but the occurrence of marine taxa can be either attributed to limited marine influences or more likely to reworking (see above).

6.1.3 Elements of chronology

It is suggested that the high level of MIS 5e (Bard et al., 1996; Koeling et al., 2009) is represented here by zones 22-D3 to 5. In the whole of MIS 5, it is mainly in the maximum sea level of MIS 5e that the Black Sea would have been connected to the Global Ocean and the Turkish Straights would have the two-way exchange of

601 water as today. It was established earlier that stratigraphic succession immediately
602 above the red-H1 reflector belongs to MIS 4 (Kende, 2018; Çağatay et al., 2019),
603 which can now be shown to reflect a brackish-Pontocaspian environment. During
604 MIS 4, the SoM was an oligotrophic lake, with no evidence of water body
605 stratification, and was almost certainly disconnected. During the late phases of MIS
606 5, the inflow of Mediterranean water was restricted and this probably required a
607 Dardanelles Sill depth higher that the present sill depth. We will come back to this
608 point in the discussion and here only consider the phasing of the marine to brackish
609 transition. In the age model proposed in Çağatay et al. (2019), this transition occurs
610 after MIS 5d (in the 110 to 100 ka interval) at a time of sea-level rise, and that may
611 be considered unlikely. This transition more probably occurred concurrently with sea-
612 level drop either later in MIS 5c or during the transition from MIS 5e to 5d. Assigning
613 this transition to later in MIS 5c would keep the sapropel correlation proposed by
614 Çağatay et al. (2019) but imply that MIS 5d is not observed in the pollen record in
615 either core (Leroy et al., submitted).

616 6.2 Core CS18: taphonomy, surface water condition and chronology

617 *6.2.1 Taphonomy*

618 Before the transition 18D-2 to 3 (756 cm) towards marine assemblages, thus
619 already at the beginning of pollen zone 18P-2 (786.5-730.5 cm), one may see
620 sudden changes. This is firstly a sediment change from homogenous to finely
621 laminated around 772 cm and two round pebbles (of river origin?) are found at 775
622 and 758.5 cm, in between them one finds a 2 mm-thick silt layer (773 cm). Moreover,
623 at 771 cm a sharp increase of the concentration in pollen and spores (from <5000 to
624 > 25,000 palynomorphs/ml) and at 762 cm a sharp and long-lasting reduction of the

reworked pollen. The sharp statistical limit at 756 cm in the dinocyst diagram is 17 cm above the 2 mm-thick silt layer. These observations are in support of an increase of water level with the influx of marine water from the Aegean Sea (Çağatay et al., 2009) leading to sediment disturbance and taphonomical changes.

The dinocyst sharp limit at 570 cm is slightly above the hiatus at 580 cm (one sample). It is interesting to note here the absence of the equivalent to zone 22D-4 with its very high percentages of cysts of *P. dalei* and *S. trifida*. The sediment in core CS 18 was probably lost by erosion linked to this hiatus.

In general, dinocysts and pollen are well preserved in the three sapropels and their concentrations are maximal, as observed in core CS22. Minimal concentrations are reached in MIS6 and 4.

After the red-H1 hiatus, a barren sample (neither pollen, nor dinocysts, but many *Dreissena* shell debris) is noted. In the following sample, a peak of *L. machaerophorum*, a large peak of reworked pollen, significant presence of reworked dinocysts and abundance of *Glomus* co-occur. Therefore, no marine invasion can be reconstructed; to the contrary a strong coastal, even soil, input should be recognised. The sediment taphonomy changes completely.

6.2.2 Sea-surface conditions

The transition from brackish Pontocaspian to fully marine conditions (zones 18D-2 to 3, main change highlighted by CONISS) seems to occur very abruptly at 756 cm depth (Fig. 4 and 7). Then in zone 18D-3, the conditions are only fully marine. Zone 18D-4 is a transitional period, back towards a brackish-Pontocaspian environment. This transition zone is also well marked in the NMDS results (see green arrow in Fig. 8). The surface waters of subzone 18D-5a are clearly brackish-Pontocaspian. Subzone 18D-5b is mostly brackish-Pontocaspian but some

influences from the sea are felt, although as in core CS22 a taphonomical impact is very important. Below 756 cm, the assemblages of zones 18D-1 and 2 are brackish-Pontocaspian, with significant reworking in zone 18D-1 both in dinocysts and in pollen.

The group of dinocysts reflecting warm SST (Fig. 4 and 7) is especially abundant in zone 18-D3. The presence of *B. tepikiense*, as in the CS22 core, indicates seasonal temperature contrast at that time.

Two large peaks of *L. machaerophorum* are noted just above a hiatus, i.e. at the base of zone 18D-3 and at the base of zone 18D-5b. After the transition from zone 18D-2 to 3, a peak of cysts of *S. trifida* is also present. Both taxa are signs of nutrient enhancement.

The P/D ratio fluctuates throughout the record. One may note however high values in subzone 18-D1a and at the base of zone 18-D4. The values are especially low in the middle of zone 18D-3, suggesting high water levels.

6.2.3 Elements of chronology

Zones 18D-3 (marine taxa and low P/D) and 18D-4 (transition) reflect the MIS 5e high sea levels. The warm-loving taxa are present in the same zone and confirm interglacial conditions as deduced from pollen analysis. However, it is likely that this zone is not complete as a characteristic dinozone in core CS22 (high percentages of cysts of *P. dalei* and cysts of *S. trifida*) is missing from it (Leroy et al., submitted).

Zones D18-1 and 2 are suggested to represent low water levels and, if the sequence is in continuity, glacial stage MIS 6. As a reminder, above the red-H1 hiatus, brackish conditions have previously been related to MIS 4 (Kende, 2018; Çağatay et al., 2019).

In conclusion, the chronology proposed here represents an in-depth revision of that in Çağatay et al. (2019), with especially the occurrence of a larger part of MIS 5e and of MIS 5c and fits the chronology based on geochemistry and pollen analysis proposed in Leroy et al. (submitted).

6.3 Comparison of the dinocyst records within the Sea of Marmara and to the Black Sea

6.3.1 Diversity

The dinocyst assemblages are similar in core CS22 and core CS18, with slightly more marine taxa in CS22 and brackish-Pontocaspian taxa in CS18, reflecting the difference in the extension of glacial versus interglacial periods covered in the two sequences (Table SI3). The total number of taxa is larger in core CS18; the latter because of the long MIS 6 record. Taxa at play in core 22-GC3 in the SE Black Sea are similar to those in the two Marmara cores, although the Black Sea seems to have more heterotrophic cyst diversity and the SoM more brackish-Pontocaspian taxon diversity (Table SI3). Modern and Holocene records across the Black Sea show geographic differences in the distribution of heterotrophic taxa (Mudie et al., 2017). This may be due to variations in water turbidity, limitations to photosynthesis, or possibly competition with other phytoplankton groups. Remarkably, *S. inaequalis* and *S. trifida* are two particularities of the SoM versus the Black Sea.

6.3.2 MIS 5e

In core 22-GC3 (SE Black Sea), the transition from brackish Pontocaspian to marine conditions during MIS 5e is dated at 128 ka (Shumilovskikh et al., 2013). The change is progressive contrary to that in core CS18, underlining the possibility of a

hiatus in core CS18 at the beginning of the marine phase (see the earlier taphonomy section) linked to flooding by marine waters. The subsequent peak of nutrients in core CS18 is possibly due to shore erosion as sea level rose. The very high percentages of cysts of *P. dalei* and *S. trifida* in zone 22D-4 find no equivalent in core CS18. The transition from marine to brackish (mixed assemblages) is made over 20 cm only within zone 22D-5, whereas it is much longer in core CS18 (zone 18D-4, 70.5 cm). These two observations suggest other significant hiati and deeper waters in the west that were invaded quickly by saline waters.

In the middle of the marine phase, a *Pinus* zone (22P-2, 2042-1982 cm depth, and 18P-6, 621-581 cm depth) has been recognised in both cores and quantitative climatic reconstruction (based on pollen) proposed a cool-humid climate not suggestive of a stadial steppe (Leroy et al., submitted). Due to the presence of the warm-loving dinocysts before, during and after, this mid-Eemian phase thus has an ambiguous interpretation. A continental climate in the *Pinus* zone underlined by the presence of seasonal contrast dinocyst assemblages is nevertheless likely.

The end of the marine phase is not presented in core 22-GC3 due to a turbidite (Wegwerth et al., 2018). The end of the marine phase may however be studied in the two Marmara cores here and seems to have been progressive with a period when the two types of dinoflagellate assemblages co-existed (zones 22D-5 and 18D-4), i.e. marine and brackish.

It is noteworthy to underline the peaks of *S. trifida* both at the beginning of the marine phase (zone 18D-3a) and at the end of it (zone 22D-4), in both cases attributed to fluctuating salinities between marine and brackish-Pontocaspian. At the end of the marine period in core CS22, in addition, the high values of cysts of *P.*

722 *dalei* may be attributed to terrigenous input, probably related to water level lowering,
723 as proposed for the Holocene (Verleye et al., 2009).

724 The widely-spaced analyses on core DSDP Site 380 sampled a weakly
725 marine phase as the occurrence of brackish dinocyst taxa (58%) is quite substantial
726 (Ferguson et al., 2018). A diagram from DSDP Site 379A has one sample in MIS 5e
727 (Hoyle et al., 2021). This unique spectrum shows abundance of *L. machaerophorum*
728 with long processes, *Spiniferites* sp. and some marine taxa. The $^{87}Sr/^{86}Sr$ ratio
729 supports a marine connection at that time. The interglacial periods in the Gulf of
730 Corinth were generally marine as Global Ocean level is high. In the lithostratigraphic
731 unit correlated to MIS 5, the surface water conditions were generally warmer as
732 established by similar warm-loving species to those found in the SoM (Fatourou et
733 al., 2023).

734 *6.3.3 MIS 6 and 4*

735 The NMDS analysis shows that MIS 6 and MIS 4 dinocyst assemblages are
736 clearly different, although both brackish-Pontocaspian (Fig. 8), i.e. more *P. psilata*
737 and clear presence of *S. inaequalis* and *Caspidinium* in MIS 6, contrasted with more
738 *S. cruciformis* in MIS 4. Some common points are noted between the MIS 6 and MIS
739 4 assemblages of the current study and the MIS 3 assemblages of other Marmara
740 cores (Mudie et al., 2004): all show a mix of dominant brackish-Pontocaspian
741 dinocysts with some marine ones and all have low to very low cyst concentrations.
742 The latter may be due to high sedimentation rates diluting the fossil content. Erosion
743 is active in glacial stages, as seen by the percentages of reworked elements that are
744 very high in the MIS 6 of core CS18 and in the MIS 4 of cores CS22 and CS18.
745 Other investigators often do not count them, neither published them, but they are a
746 significant indicator of erosion and inwash. Often reworking also shows proximity to

shores due to low water level. The water level must have been relatively low, most likely lower than at any time in MIS 5. The brackish-Pontocaspian periods during MIS 5 are clearly different from those of MIS 6 and 4, in that the latter ones have a lot of reworking and contain abundant signs of erosion (Fig. 3, 4 and 8).

Core CS18 in the Imralı basin is not far from the North Imralı canyon that the Kocasu carved during lowstands (Çağatay et al., 2015a and b). This relative proximity to a river (if not to the shore) and submarine canyon may also explain the high amounts of reworked elements and the different taphonomy during the glacial times (Pope et al., 2022).

It is very likely that, as suggested in Hoyle et al. (2021) based on Sr ratio in the Black Sea, no marine connection occurred during the glacial periods for the SoM. Several indicators (oxygen isotopes of the Sofular Cave along the Turkish coast of the Black Sea (Badertscher et al., 2011) and Sr isotope ratio (Hoyle et al., 2021)) suggest an overflow from the Caspian Sea to the Black Sea during MIS 6. Unfortunately, dinocyst assemblages cannot contribute evidence to this debate on water source.

For MIS 6, a progressive, even slow, freshening after marine conditions in the previous interglacial (MIS 7) was suggested on the basis of divergent trends in isotopic values, i.e. $\delta^{18}O$ becomes more negative while $\delta^{13}C$ becomes more positive (Çağatay et al., 2009). This may explain why here the marine dinocyst group is better represented in subzone 18D-1a than subzones 18D-1b and c, even 18D-2. This also suggests that the base of the core may have just missed the top of MIS 7. As a significant contribution of reworking of marine palynomorphs (as shown here) is revealed, no marine connection would have occurred during MIS 6 (zones 18D-1 and 2). For that matter, at the transition from the marine phase to the lake phase at

MIS 5 to 4, Grall et al. (2014) and Aziz et al. (2019) suggest slope failure and strong turbidity currents entraining sediment that was stored on the shelf to deeper areas of the SoM, as the sea level fell. Recent investigations (modern discharge and geological data) aiming at disentangling the origin of the sediment in the SoM during low levels have however demonstrated that southern river input was more important than suspended load through one or both straits (Hiscott et al., 2021). Moreover, the latter authors further estimate that river input was higher than mass-wasting events and shoreface erosion. Nowadays, and most likely in the past, the Kocasu is the largest southern river and it drains a large basin in NW Anatolia (Kazancı et al., 2004).

The water levels in the Black Sea were most likely low during the cold parts of MIS 6. However, three major meltwater pulses of the Eurasian icesheets occurred; but it is not known if the lake level rise of the Black Sea was sufficient to cause an overspill to the SoM although it is likely (Wegwerth et al., 2019). So far these pulses cannot be seen in our record. For completeness of the record, it is noteworthy to underline that the glacials (MIS 6 and 4) in the Gulf of Corinth were generally brackish (Fatourou et al., 2023).

6.4 Sapropels

6.4.1 Surface conditions and sapropel formation

The sapropels deposited in SoM during MIS-5 clearly formed under three different surface water conditions (Fig. 7). MSAP-2 formed under brackish surface conditions (except briefly on a few cm within MSAP 2b), MSAP-4 under clearly marine surface conditions and MSAP-3 in a period of transition from marine to brackish surface conditions.

Although not a perfect fit, the dinocyst concentration increases in each sapropel. Admittedly dinocysts are only one part of the bloom-forming phytoplankton, diatoms being the main group. In order to appreciate the amount of other phytoplankton such as diatoms, the H/A ratio is used as an indicator of primary productivity, as heterotrophic dinoflagellate prey on diatoms (see Triantaphyllou et al., 2009; Sala-Perez et al., 2020). The results show higher H/A ratio, thus higher palaeoproductivity, during the marine phase in MIS 5e in core CS18, especially in MSAP-4 (Fig. 9). The diatom assemblages (only available for MSAP-2 in core CS22) are freshwater-brackish. This H/A ratio is low in MSAP-2b, suggesting low productivity.

The origin of the sapropel formation in the SoM, the decreasing surface salinities and the decrease of the oxic condition at bottom over MIS 5 may be the reason why palaeoproductivity based on the H/A ratio is clearly higher in MSAP-4 only.

6.4.2 Bottom conditions and sapropel formation

In core CS22 below MSAP-3, the gradual shift of foraminifera assemblages, starting with genera needing oxic conditions towards suboxic-tolerant genera, is an effect of oxygen loss caused by the formation of water column stratification and organic matter mineralisation (Fig. 9). It is worth noting that the occurrence of foraminifera linings is only in the marine period. Accordingly in the marine phase of core CS22, the linings occur from the core base and stop at the beginning of the sapropel MSAP-3 at 1920 cm. Their occurrence is similar to that of the foraminifera shells (Fig. 9).

In contrast, in core CS18, foraminifer linings are present at 725.5-605.5 and 564.5-524.5 cm depth, thus in sapropels MSAP-4 and 3. Moreover foraminifer shell

distribution (Çağatay et al., 2019) (Fig. 9) is like that for the linings, although somewhat shorter. In core CS18, shells are found in the first part of MSAP-4 and between MSAP-4 and 3.

This foraminifera distribution in the sapropels is therefore questioning the existence of full anoxia in MSAP-4 (core CS18) and in part of MSAP-3 (mostly in core CS18, no foraminifera in core CS22). For MSAP-2, it is unclear whether the deep water remained sufficiently saline for benthic foraminifera to live.

6.4.3 Sapropel trigger in the Sea of Marmara

Combining the information from bottom and surface conditions (especially dinocysts, foraminifera shells and organic linings), it may be shown that the four Marmara sapropels (4, 3, 2b and 2a) clearly formed over times with decreasing marine influence and increasing stratification. Moreover they are different from each other. Only MSAP-2 may have had fully anoxic conditions during the whole sapropel time.

The difference between the two cores may be possibly explained by the shallower position of core CS18 in comparison to core CS22. The water depth difference is 260 m, adding another c. 14 m (at the end of MSAP-3) due to core depth difference, thus a total of c. 274 m difference (Fig. 9). The location of the shallower core CS 18 would make it harder to fall within the depths affected by full anoxia and would justify the occurrence of foraminifera in MSAP-4 and 3 in a dysoxic area. Our results also show that the anoxia did not rise up to 291 m water depth. In the east Mediterranean Sea, sapropels S5 (MIS5e) and S6 (MIS 6e) contained foraminifera. It is interesting to note that during MSAP-1 suboxic conditions extended over the shelf to depths of -75 m (Çağatay et al., 2009). These results (and the difference between cores CS22 and CS18) may be important to further understand

anoxia (or euxinia) development during the Eemian sapropel formation in the Black Sea, where it has been shown to be stronger than the Holocene one (Wegwerth et al., 2018).

The Marmara sapropels occur during warm periods, evidenced in the current joint pollen-dinocyst investigation i.e. Eemian, Saint-Germain I and II, which more likely facilitated algal blooms. Consequently, the proposed correlation between the Marmara sapropels and the Mediterranean sapropels becomes: MSAP-4 – S5, MSAP-3 – S5 too, MSAP 2b – S4 and MSAP-2a – S3 (Fig. 9), based on ages (Grant et al., 2016). The Marmara sapropels do not seem to be preconditioned by astronomical forcing as for the Mediterranean ones (Rohling et al., 2015; Grant et al., 2016). Thus further to the astronomical cause of sapropel formation in the Mediterranean Sea, other sapropel formation triggers may be sought for the SoM. A specific trigger mechanism in the SoM is an inflow of marine water causing water column stratification (Çağatay et al., 2009).

6.5 Terrestrial and marine transitions in the Marmara and the Black seas

Understanding the facies transitions in the SoM or Lake requires taking into account the hydrodynamic processes and how they control sediment deposition and erosion in the straights. Obviously, the outflow from the Black Sea to the Sea of Marmara is governed by river inputs to the Black Sea and evaporation/precipitation. When the water budget of the Black Sea is positive, it will inevitably overspill into the SoM and then most likely into the Mediterranean Sea as the SoM has a comparatively small surface area for evaporation. On the other hand, the occurrence of a counter current of sea water from the Mediterranean Sea to the SoM when sea level is above the Dardanelles Straight and to the SoM to the Black Sea when sea level is above the Bosphorus Sill cannot be taken for granted. For instance, in the

present day with a sill depth of -35 m in the Bosphorus Straight, the seawater bottom current is blocked when the surface current exceeds 30,000 $m^3.s^{-1}$ (Sannino et al., 2017). This situation occurs during transient events in the present conditions, but more generally the hydrodynamics of the straights implies that the influx of seawater is a function of water depth at the sill and of the freshwater outflow, which is in turn governed by river inputs and evaporation/precipitation. Moreover, in steady state, the only way out for seawater entering the Dardanelles Straight is by mixing with the fresher surface water layer in the SoM or in the Black Sea. In the present day, and considering yearly averages, the bottom current flux through the Dardanelles Straight is only about 12 % larger than the bottom current flux through the Bosphorus Straight (Beşiktepe et al., 1994). It follows that the halt of northward flux through the Bosphorus Straight would also greatly reduce the seawater flux into the SoM and thus increase the residence time of the SoM bottom water. The residence time of deep water in the SoM varies from two years in the Tekirdag and the Central Basin to 10-20 years in Çınarcık Basin (Beşiktepe et al., 1994), and this causes an eastward decrease of oxygen concentration from 60 to 8 µmol l^{-1} (Henry et al., 2007). Increasing the residence time will further reduce oxygen content, which may in turn favour sapropel deposition.

Variations of sill elevation depend on tectonic movements, erosion and sedimentation. The shores of the Dardanelles Straight have been uplifting at a rate estimated in the 0.25-0.75 mm yr^{-1} range (Yaltırak et al., 2002). This may suggest that the level of the sill has risen with time. However, the Dardanelles Straight is at least in part structurally controlled (Yaltırak et al., 2000; Gökaşan et al., 2008) and active faults along part of its shore may locally cause subsidence of the channel floor. Two sedimentary units have been deposited on an erosional surface cutting

through Miocene and Pliocene sediments and their geometry gives clear indications on the erosion and sedimentation processes (Gökaşan et al., 2008). The lower unit is thickest (up to 80 m) at the mouths of rivers discharging in the Dardanelles Straight where they formed deltas that were subsequently incised. The upper unit is composed of Holocene sediment drifts that are thickest where the channel is wide and are incised by the active bottom current in the narrow parts. It thus appears that the strength of the bottom current in the Dardanelles Straight, which is in the present-day conditions controlled by the dynamics of the Bosphorus Straight, redistributes sediments and prevents clogging of the channel. All the above observations and reasoning leads to hypothesize that the interruption of the northward flux through the Bosphorus Straight leads to the restriction of the Dardanelles channel by deltas forming at the mouths of local rivers. In the Dardanelles Straight, the current sill depth is defined by the top of Unit I at -65 m while the basement sill is at -85 m and in the Bosphorus Straight, the present-day sill depth is at -35 m while the basement sill is at -70 m (Çağatay et al., 2009).

In core CS18, the brackish to marine transition occurs still within the Saalian Glacial (c. MIS 6), i.e. before the development of the thermophilic vegetation of the Eemian Interglacial. Moreover, the end of the marine phase occurs before the end of Eemian Interglacial in both cores. This offset is in line with the observation that the Eemian Interglacial and the MIS 5e are not exactly synchronous, with the Global Ocean level rising first, followed by vegetation changes (Shackleton et al., 2003).

In the SE Black Sea (core 22-GC3), the marine influence however starts only at 128 ka (or 815.5 cm depth) between *Quercus-robur*-type zone (22GC-E1) and the *Juniperus* zone (22GC-E2), i.e. well into the interglacial (Shumilovskikh et al., 2013); whereas here in core CS18 it starts earlier at 756 cm depth, i.e. in the middle of zone

18P-2 dominated by *Artemisia* and that is probably still part of the Saalian Glacial. Although a large difference between the SoM and the Black Sea palynological diagrams, this can be explained by the marine inflow that has first to penetrate the SoM from the Aegean Sea and cross two sills, before reaching the Black Sea. For comparison, a delay of 4-6 ka has been observed for the Lateglacial-Holocene, with a marine incursion in the SoM starting at 14.7 ka followed by progressive salinisation with a facies transition defined at 12.6 ka (Vidal et al., 2010; Çağatay et al., 2015) and in the Black Sea at 8.9-8.3 ka (Shumilovskikh et al., 2013; Mudie et al., 2014; Yakupoğlu et al., 2022). This lag has been explained by the difference in sill depth between the Bosphorus and the Dardanelles Straights, the Bosphorus one being close to its present-day level (-35 m) at the time of reconnection and the Dardanelles one being somewhat deeper (-75 ± 5 m) than its present-day level. The situation during the MIS 6 to 5 transition may have been similar with a Bosphorus Straight at about -40 m (Çağatay et al., 2019). The early marine incursion in the SoM at the end of MIS stage 6 indicates that the Dardanelles sill depth was also deeper at that time.

A new result from the present study that remains to be explained is the prevalence of brackish Ponto-Caspian conditions in surface water during the later phases of MIS 5 at times when sea level was well above the present-day Dardanelles sill level (Fig. 9). The explanation we propose is that the Bosphorus northward flow was first decreased then interrupted as sea level started decreasing before the end of MIS 5e, and that resulted in a progressive reduction of seawater inflow through the Dardanelles Straight. This decreased oxygen availability in the marine deep waters, as indicated by foraminifer assemblages, eventually enabled the sediment filling of the channel by local rivers, further limiting marine input. Low and/or episodic sea-water inputs during the later part of MIS 5 may have maintained

stratified conditions in the SoM with low salinity surface waters and nearly anoxic bottom water of intermediate salinity. Sea level drop during MIS 5d and 5b presumably interrupted the marine inflow, lowering the vertical salinity contrast and allowing better oxygenation of the deep waters. During the following glacial lowstands (MIS 4-3-2), the Marmara lake remained isolated and outflow (either permanent or episodic) may have incised the sedimentary deposits to allow reconnection at ≈-75 m at the end of the glaciation.

The $\delta\ ^{18}O$ of the well-dated Sofular stalagmite record reflects salinity of the Black Sea surface waters by way of evaporation and moisture availability (Badertscher et al., 2011). These authors propose one clear period of connection between the Black Sea and the Mediterranean Sea at roughly MIS 5e based on a threshold of -8.5± 1‰ $\delta\ ^{18}O$ values. The next period below that threshold is at MIS 5c and also suggests connection but for a shorter period. The last period at MIS 5a would not have led to sufficiently high water levels to allow flowing of the Mediterranean marine waters into the Black Sea. This fits rather well our results in the SoM, with a full surface water connection at MIS 5e when global sea level reached 8 m above sea level, a marine incursion affecting surface waters during MIS 5c when global sea level reached 24 m below sea level and no incursion during MIS 5a when global sea level reached only 28 m below sea level (Rohling et al., 2021).

7 Conclusions

The results of this investigation have shown the widely changing states of the Sea of Marmara during the MIS 6 and 5, implying vastly changing connexions with the Pontocaspian basin and the Global Ocean.

From the methodological point of view, as for the Caspian Sea (Leroy et al., 2013, 2014) when using the palynological method (pollen and dinocysts), it is essential to study separately and objectively the terrestrial conditions and the aquatic ones. A comparison of the two approaches may then clearly demonstrate if the changes are synchronous or not, and if different forcing factors are at play.

As demonstrated for the Iberian margin by pollen and isotopic analyses, the Eemian starts and finishes respectively after the start and after the end of MIS 5e high levels. The same offset can be demonstrated here in this joint pollen - dinocyst study.

The combination of the two sequences, CS22 and CS18, following the chronology proposed in Leroy et al. (submitted), allows highlighting one main marine phase corresponding to MIS 5e (marine surface and bottom conditions) and a minor one (mixed surface conditions) in MIS5c. The rest of the record is brackish-Pontocaspian although with some differences across the sequence (e.g. MIS 6 versus MIS 4). Based on climatic data (pollen) allowing linking the records, a delay in the marine influence between SoM and SE Black Sea is observed, perhaps due to the closure of the Bosphorus Sill and its late opening or a different sill height.

The current water level reconstruction corresponds well to the Global Ocean level curve and Black Sea salinity reconstructions, both indicating progressively lower high stands (i.e. from MIS 5e to 5a) and decreasing connections between the Black Sea and the SoM across MIS 5.

The four sapropels (MSAP-4, 3, 2a and 2b) formed under very different surface water conditions ranging from marine to brackish-Pontocaspian, but always under a warm climate. Moreover, the shallower site (CS18) in the east (Imralı basin) does not form as often full anoxia than the western and deeper site (CS22). For

example: the top limit of the bottom anoxia in sapropel MSAP-4 would not have reached 291 m water depth (location of core CS18).

In the future, it would be interesting to apply palynological investigations (pollen and dinocysts) on long cores on both sides of the Bosphorus Strait to define better for example the timing difference for the marine reconnection at the boundary MIS 6-5.

Acknowledgements

We are grateful to Jennifer Bradley and Luke Glascott at the University of Liverpool (UK) and Dahvya Belkacem at IMBE (Aix-en-Provence, France) for palynological extraction in the pollen laboratories. Cores were taken during the MARSITECRUISE of Ifremer/Genavir R.V. Pourquoi Pas?, within the framework of MARSITE FP7 EU Project (grant agreement no: 308417). Thanks are due to N. Çağatay, K. Eriş and N. Yakupoğlu from ITU (Turkey) who gave access to core CS18 for sampling and contributed to the improvement of this publication owing to intensive discussions over the years. Part of this work has been supported by Bilateral ANR/TÜBITAK collaborative research project MAREGAMI (ANR-16-CE03-0010-02) and Tubitak Project (116Y371).

Data availability

The dinocyst data are available in PANGEA.

References

Aydoğdu, A., Pinardi, N., Özsoy, E., Danabasoglu, G., Gürses, O, Karspeck, A., 2018. Circulation of the Turkish Straits System under interannual atmospheric forcing. Ocean Sci. 14, 999–1019.

Aziz, S., McHugh, C.M., Ryan, W.B.F., Henry, P., Kende, J., Delligatti, M., Tachikawa, K., 2019. New insights into the rapid transformation of the sea into a lake, Marmara Sea, Turkey. AGU abstract. https://ui.adsabs.harvard.edu/abs/2019AGUFMPP21D1650A/abstract

Badertscher, S., Fleitmann, D., Cheng, H., Edwards, R.L., Göktürk, O.M., Zumbühl, A., Leuenberger, M., Tüysüz, O., 2011. Pleistocene water intrusions from the Mediterranean and Caspian seas into the Black Sea. Nat. Geosci. 4, 236–239.

Balkis, N., Balci, M., Giannakourou, A., Venetsanopoulou, A., Mudie, P., 2016. Dinoflagellate resting cysts in recent marine sediments from the Gulf of Gemlik (Marmara Sea, Turkey) and seasonal harmful algal blooms. Phycologia 55, 2, 187–209

Bard, E., Jouannic, C, Hamelin, B., Pirazzoli, P., Arnold, M., Faure, G., Sumosusastro, P., Syaefudin, 1996. Pleistocene sea levels and tectonic uplift based on dating of corals from Sumba Island, Indonesia. Geoph. Res. Lett. 23, 12, 1473-1476.

Bennett, K., 2007. Psimpoll and Pscomb Programs for Plotting and Analysis. Version Psimpoll 4.27. http://chrono.qub.ac.uk/psimpoll/psimpoll.html (accessed 27 May 2020).

Beşiktepe, S.T., Sur, H.I., Özsoy, E., Latif, M.A., Oğuz, T., Ünlüata, Ü., 1994. The circulation and hydrography of the Marmara Sea. Prog. Oceanogr. 34, 285–334.

1037 Bradley, L.R., Marret, F., Mudie, P.J. et al., 2012. Constraining Holocene sea-
1038 surface conditions in the south-western Black Sea using dinoflagellate cysts.
1039 Journal of Quaternary Science 27, 835–843.
1040 Bravo, I., Figueroa, R.I., 2014. Towards an ecological understanding of dinoflagellate
1041 cyst functions. Microorganisms, 2, 11–32.
1042 Çağatay, M.N, Görür, N., Algan, A, Eastoe, C.J., Tchapalyga, A., Ongan, D., Kuhn,
1043 T, Kuşcu, İ., 2000. Late Glacial-Holocene palaeoceanography of the Sea of
1044 Marmara: timing of connections with the Mediterranean and the Black
1045 Sea. Marine Geology 167, 191-206.
1046 Çağatay, M.N., Eriş, K., Ryan, W.B.F., Sancar, Ü., Polonia, A., Akçer, S., Biltekin, D.,
1047 Gasperini, L., Görür, N., Lericolais, G., Bard, E., 2009. Late Pleistocene–
1048 Holocene evolution of the northern shelf of the Sea of Marmara. Marine Geology
1049 265, 87–100.
1050 Çağatay, M.N., Wulf, S., Sancar, Ü., Özmaral, A., Vidal, L., Henry, P., Gasperini, L.,
1051 2015a. The tephra record from the Sea of Marmara for the last ca. 70 ka and its
1052 palaeoceanographic implications. Mar. Geol. 361, 96-110.
1053 Çağatay, M.N., Uçarkuş, G., Eriş, K.K, Henry, P., Gasperini, L., Polonia, P., 2015b.
1054 Submarine canyons of the Sea of Marmara. In CIESM Monograph 47 [F. Briand
1055 ed.] Submarine canyon dynamics in the Mediterranean and tributary seas- An
1056 integrated geological, oceanographic and biological perspective, pp. 123- 135.
1057 CIESM Publisher, Monaco.
1058 Çağatay, M.N., Eriş, K.K., Makaroglu, Ö., Yakuboğlu, N., Henry, P., Leroy, S.,
1059 Uçarkuş, G., Sakınç, M., Yalamaz, B., Bozyiğit, C., Kende, J., 2019. The Sea of
1060 Marmara during Marine Isotope Stages 5 and 6. Quat. Sc. Rev. 220, 124-141.

Çağatay, M.N., Eriş, K.K., Erdem, Z., 2022. Morphology and Late Pleistocene-Holocene Sedimentation of the Strait of İstanbul (Bosphorus): A review. In: Rossi, V. M., Longhitano, S., Olariu, C. and Chiocci, F. (eds) Straits and Seaways: Controls, Processes and Implications in Modern and Ancient Systems. Geological Society, London, Special Publications, 523, https://doi.org/10.1144/SP523-2021-48.

Cheddadi, R., Rossignol-Strick, M., 1995. Improved preservation of organic matter and pollen in eastern Mediterranean sapropels. Paleoceanography 10, 2, 301-309.

Chepalyga, A.L., 2007. The late glacial great flood in the Ponto-Caspian basin. in: Yanko-Hombach, V., Gilbert, A.S., Panin, N., Dolukhanov, P.M. (Eds), The Black Sea Flood Question. Springer, pp. 119-148

Clarke, K.R., Gorley, R.N., 2015. PRIMER v7: User Manual/Tutorial. PRIMER-E, Plymouth (296 pp.).

Cornuault, M., Vidal, L., Tachikawa, K., Licari, L., Rouaud, G., Sonzogni, C., Revel, M., 2016. Deep water circulation within the eastern Mediterranean Sea over the last 95 kyr: New insights from stable isotopes and benthic foraminiferal assemblages. Palaeogeography, Palaeoclimatology, Palaeoecology 459, 1–14.

de Vernal, A., 2009. Marine palynology. IOP Conf. Ser.: Earth Environ. Sci. 5 012002.

de Vernal, A., Marret, F., 2007. Organic-Walled Dinoflagellate Cysts: Tracers of Sea-Surface Conditions. Development in Marine Geology 1, 371-408.

de Vernal, A., Radi, T., Zaragosi, S., Van Nieuwenhove, N., Rochon, A., Allan, E., De Schepper, S., Eynaud, F., Head, M.J., Limoges, A., Londeix, L., Marret, F., Matthiessen, J., Penaud, A., Pospelova, V., Price, A., Richerol, T. 2020.

Distribution of common modern dinoflagellate cyst taxa in surface sediments of the Northern Hemisphere in relation to environmental parameters: The new n=1968 database. Marine Micropaleontology, art. no. 101796.

Eriş, K.K., Ryan, W.B.F, Çağatay, M.N., Sancar, U., Lericolais, G., Menot, G., Bard, E., 2007. The timing and evolution of the post-glacial transgression across the Sea of Marmara shelf south of İstanbul. Marine Geology 243, 1-4, 57-76.

Eriş, K.K., Çağatay, M.N., Akçer, S., Casperini, L., Mart, Y., 2011. Late glacial to Holocene sea-level changes in the Sea of Marmara: new evidence from high-resolution seismics and core studies.Geo-Marine Letters 31, 1, 1-18.

Fatourou, E., Kaftzidou, A., Marret, F., Panagiotopoulos, K., Kouli, K., 2023. Late Quaternary Ponto-Caspian dinoflagellate cyst assemblages from the Gulf of Corinth, Central Greece (eastern Mediterranean Sea). Marine Micropal. 179, 102211.

Ferguson, S., Warny, S., Escarguel, G., Mudie, P.J., 2018. MIS 5e1 dinoflagellate cyst analyses and morphometric evaluation of *Galeacysta etrusca* and *Spiniferites cruciformis* in southwestern Black Sea. Quaternary International 465, 117-129.

Gökaşan, E., Ergin, M., Özyalvaç, M., Sur, H.I., Tur, H., Görüm, T., Ustaömer, T., Batuk, F.G., Alp, H., Birkan, H., Türker, A., Gezgin, E., Özturan, M., 2008. Factors controlling the morphological evolution of the Çanakkale Strait (Dardanelles, Turkey). Geo-Mar. Lett. 28,107–129.

Gökaşan E., Tur, H., Ecevitoglu, B., Görüm, T., Türker, A., Tok, B., Çaglak, F., Birkan, H., Simşek, M., 2005. Evidence and implications of massive erosion along the Strait of Istanbul (Bosphorus). Geo-Mar. Lett. 25, 324–342.

Grall, C., Henry, P., Westbrook, G.K., Cagatay, MN, Thomas, Y., Marsset, B., Borschneck, D., Saritas, H., Cifçi, G., Géli, L., 2014. Mass transport deposits

periodicity related to glacial cycles and marine-lacustrine transitions on a ponded basin of the Sea of Marmara (Turkey) over the last 500 ka. Chapter 53. In: Krastel, S. et al. (eds) Submarine mass movement and their consequences. Advances in Natural and Technological Hazards Research 37, Springer International Publishing Switzerland, pp. 595-603.

Grant, K.M., Grimm, R., Mikolajewicz, U., Marino, G., Ziegler, M., Rohling, E.J., 2016. The timing of Mediterranean sapropel deposition relative to insolation, sea-level and African monsoon changes. Quaternary Science Reviews 140, 125-141.

Head, M.J., Lewis, J., de Vernal A., 2006. The cyst of the calcareous dinoflagellate *Scrippsiella trifida*: resolving the fossil record of its organic wall with that of *Alexandrium tamarense*. Journal of Paleontology 80, 1, 1-18.

Henry, P., Şengör, A.M.C., Çağatay, M.N., 2007. MARNAUT cruise, RV L'Atalante. https://doi.org/10.17600/7010070.

Hiscott, R.N., Aksu, A.E., Yaltırak, C., 2021. The uppermost Pleistocene–Holocene mud drape across the Marmara Sea: Quantification of detrital supply from southern Marmara rivers. Sedimentary Geology 415, 105851.

Hoyle, T., Bista, D., Flecker, R., Krijgsman, W., Sangiorgi, F., 2021. Climate-driven connectivity changes of the Black Sea since 430 ka: Testing a dual palynological and geochemical approach. Palaeogeography, Palaeoclimatology, Palaeoecology 561, 110069.

Karabanov, E.B, Prokopenko, A.A., Williams, D.F., Khursevich, G.K., 2000. Evidence for mid-Eemian cooling in continental climatic record from Lake Baikal. Journal of Paleolimnology 23, 365–371.

1134 Kazancı, N., Leroy, S., Ileri, Ö., Emre, O., Kibar, M., Öncel, S., 2004. Late Holocene
1135 erosion in NW Anatolia from sediments of Lake Manyas, Lake Ulubat and the
1136 southern shelf of the Marmara Sea, Turkey. Catena 57, 277-308.
1137 Kende, J., 2018. Tectonique et hydrologie en mer de Marmara : Histoire de
1138 l'ouverture de la mer de Marmara et reconstitution de la réponse hydrologique aux
1139 variations climatiques depuis le dernier interglaciaire. Thèse de doctorat, Aix-
1140 Marseille Université. 18 pp.
1141 Koeling, M., Webster, J.M., Camoin, G., Iryu, Y., Bard, E., Seard, C., 2009. SEALEX
1142 — Internal reef chronology and virtual drill logs from a spreadsheet-based reef
1143 growth model. Glob. Planet. Ch. 66, 149-159.
1144 Kotthoff, U., Pross, J., Müller, U. C., Peyron, O., Schmiedl, G., Schulz, H., Bordon,
1145 A., 2008. Climate dynamics in the borderlands of the Aegean Sea during
1146 formation of sapropel S1 deduced from a marine pollen record. Quaternary
1147 Science Reviews 27, 832–845.
1148 Leroy, S.A.G., Marret, F., Giralt, S., Bulatov, S. A., 2006. Natural and anthropogenic
1149 rapid changes in the Kara-Bogaz Gol over the last two centuries by palynological
1150 analyses. Quaternary International 150, 52-70.
1151 Leroy, S.A.G., 2010, Palaeoenvironmental and palaeoclimatic changes in the
1152 Caspian Sea region since the Lateglacial from palynological analyses of marine
1153 sediment cores. Geography, Environment, Sustainability, Faculty of Geography
1154 of Lomonosov Moscow State University and by the Institute of Geography of
1155 RAS. 2, 32-41.
1156 Leroy, S.A.G., Tudryn, A., Chalié, F., López-Merino, L., Gasse, F., 2013. From the
1157 Allerød to the mid-Holocene: palynological evidence from the south basin of the
1158 Caspian Sea. Quaternary Science Reviews 78, 77-97.

1159 Leroy, S.A.G., López-Merino, L., Tudryn, A., Chalié, F., Gasse, F., 2014. Late
1160 Pleistocene and Holocene palaeoenvironments in and around the Middle
1161 Caspian Basin as reconstructed from a deep-sea core. Quaternary Science
1162 Reviews 101, 91-110.
1163 Leroy, S.A.G., Lahijani, H., Crétaux, J.-F., Aladin, N., Plotnikov, I., 2020. Past and
1164 current changes in the largest lake of the world: The Caspian Sea. in: Mischke,
1165 S. (Ed.), Large Asian lakes in a changing world. Springer, pp. 65-107.
1166 Leroy, S.A.G., et al., submitted. Palynology, palaeoclimate and chronology of stage
1167 MIS 5 from two long cores in the Marmara Sea. QSR
1168 Lisiecki, L.E., Raymo, M.E., 2005. A Pliocene-Pleistocene stack of 57 globally
1169 distributed benthic d18O records. Paleoceanography, 20, PA1003
1170 Londeix, L., Herreyre, Y., Turon, J.-L., Fletcher, W., 2009. Last Glacial to Holocene
1171 hydrology of the Marmara Sea inferred from a dinoflagellate cyst record.
1172 Review of Palaeobotany and Palynology 158, 52–71.
1173 Margalef, R., 1958. Information theory in ecology. Gen. Syst. 3, 36–71.
1174 Marret, F., Zonneveld, K.A.F., 2003. Atlas of modern organic-walled dinoflagellate
1175 cyst distribution. Review of Palaeobotany and Palynology 125, 1–200.
1176 Marret, F., Leroy, S., Chalié, F., Gasse, F., 2004. New organic-walled dinoflagellate
1177 cysts from recent sediments of central Asian seas. Rev. Palaeobot. Palynol.
1178 129, 1–20.
1179 Marret, F., Mudie, P., Aksu, A., Hiscott, R.N., 2009. A Holocene dinocyst of a two-
1180 step transformation of the Neoeuxinian brackish water lake into the Black Sea.
1181 Quaternary International 197, 72-86.
1182 Marret, F., Bradley, L.R., Tarasov, P.E., Ivanova, E.V., Zenina, M.A., Murdmaa, I.O.,
1183 2019. The Holocene history of the NE Black Sea and surrounding areas: An

integrated record of marine and terrestrial palaeoenvironmental change. The Holocene 1–14.

Marret, F., Bradley, L., de Vernal, A., Hardy, W., Kim, S.Y., Mudie, P., Penaud, A., Pospelova, V., Price, A.M., Radi, T., Rochon, A., 2020. From bi-polar to regional distribution of modern dinoflagellate cysts, an overview of their biogeography. Mar Micropal 159, 101753.

McCarthy, F.M.G., Mudie, P.J., 1998. Oceanic pollen transport and pollen: dinocyst ratios as markers of late Cenozoic sea level change and sediment transport. Palaeogeography, Palaeoclimatology, Palaeoecology 138, 187-206.

Mertens, K. Ribeiro, S., Bouimetarhan, I., Caner, H., Combourieu-Nebout, N., Dale, B., de Vernal, A., Ellegaard, M., Filipova, M., Godhe, A., Grøsfjeld, K., Leroy, S. A. G. and co-authors, 2009. Process length variation in cysts of a dinoflagellate, *Lingulodinium machaerophorum*, in surface sediments: investigating its potential as salinity proxy. Marine Micropal 70, 54-69.

Mertens, K.N., Van Nieuwenhove, N., Gurdebeke, P.R., Aydin, H., Bogus, K., Bringué, M., Dale, B., De Schepper, S., de Vernal, A., Ellegaard, M., Grothe, A., Gu, H., Head, M.J., Heikkilä, M., Limoges, A., Londeix, L., Louwye, S., Marret, F., Masure, E., Matsuoka, K., Mudie, P.J., Penaud, A., Pospelova, V., Price, A.M., Ribeiro, S., Rochon, A., Sangiorgi, F., Schreck, M., Torres, V., Uzar, S., Versteegh, G.J.M., Warny, S., Zonneveld, K., 2018. The dinoflagellate cyst genera *Achomosphaera* Evitt 1963 and *Spiniferites* Mantell 1850 in Pliocene to modern sediments: a summary of round table discussions. Palynology 42, sup1, 10-44

1207 Mudie, P.J., Aksu, A.E., Yasar, D., 2001. Late Quaternary dinocysts from the Black,
1208 Marmara and Aegean Seas: Variations in assemblages, morphology and
1209 paleosalinity. Mar. Micropal. 43, 155-178.
1210 Mudie, P.J., Rochon A., Aksu, A.E., Gillespie, H., 2002. Dinoflagellate cysts,
1211 freshwater algae and fungal spores as salinity indicators in Late Quaternary
1212 cores from Marmara and Black seas. Mar. Geol. 190, 203-231.
1213 Mudie, P.J., Rochon, A., Aksu, A.E., Gillespie, H., 2004. Late glacial, Holocene and
1214 modern dinoflagellate cyst assemblages in the Aegean–Marmara–Black Sea
1215 corridor: statistical analysis and re-interpretation of the early Holocene Noah's
1216 Flood hypothesis. Rev. Palaeobot. Palynol. 128, 1-2, 143-167.
1217 Mudie, P., Yanko-Hombach, V., Kadurin, S., 2014. The Black Sea Dating Game and
1218 Holocene Marine Transgression. Open Journal of Marine Science 4, 1-7.
1219 Mudie, P.J., Marret, F., Mertens, K., Shumilovskikh, L., Leroy, SAG, 2017. Atlas of
1220 modern dinoflagellate cyst distributions in the Black Sea Corridor, including
1221 Caspian and Aral Seas. Mar Mic 134, 1-152.
1222 Mudie, P.J., Marret, F., Gurdebeke, P.R., Hartman, J.D., Reid, P.C., 2021. Marine
1223 dinocysts, acritarchs and less well-known NPP: tintinnids, ostracod and
1224 foraminiferal linings, copepod and worm remains. Geological Society, London,
1225 Special Publications 511, SP511-2020-2055.
1226 Paillès, C., Blanc-Valleron, M.M, Poulin, M., Crémière, A., Boudouma, O., Pierre, C.,
1227 2014. A new fossil diatom, *Entomoneis calixasini*, from the Turkish Marmara
1228 Sea sediments. Diatom Research 29, 4, 411-422.
1229 Pope, E.L., et al., 2022. First source-to-sink monitoring shows dense head controls
1230 sediment flux and runout in turbidity currents. Sci. Adv. 8, eabj3220.

1231 Rohling, E.J., Marino, G., Grant, K.M., 2015. Mediterranean climate and
1232 oceanography, and the periodic development of anoxic events (sapropels).
1233 Earth Sci. Rev. 143, 62-97.
1234 Rohling, E.J., Yu, J., Heslop, D., Foster, G.L., Opdyke, B., Roberts A.P., 2021. Sea
1235 level and deep-sea temperature reconstructions suggest quasi-stable states
1236 and critical transitions over the past 40 million years. Sci. Adv. 2021; 7.
1237 Sala-Pérez, M., Lattuada, M., Flecker, R., Anesio, A., Leroy, S.A.G.,
1238 2020. Dinoflagellate cyst assemblages as indicators of environmental
1239 conditions and shipping activities in coastal areas of the Black and Caspian
1240 Seas. Regional Studies in Marine Science 38, 101472.
1241 Sannino, G., Sözer, A., Özsoy, E., 2017. A high-resolution modelling study of the
1242 Turkish Straits System. Ocean Dynamics, 67, 397–432,
1243 https://doi.org/10.1007/s10236-017-1039-2.
1244 Schmiedl, G., Mitschele, A., Beck, S., Emeis, K.-C., Hemleben, C., Schulz, H.,
1245 Sperling, M., Weldeab, S., 2003. Benthic foraminiferal record of ecosystem
1246 variability in the eastern Mediterranean Sea during times of sapropel S5 and S6
1247 deposition. Palaeogeography, Palaeoclimatology, Palaeoecology 190, 139-164.
1248 Shackleton, N.J., Sanchez-Goñi, M. F., Pailler, D., Lancelot, Y., 2003. Marine
1249 Isotope Substage 5e and the Eemian Interglacial. Global and Planetary
1250 Change 36, 151-155.
1251 Shumilovskikh, L.S., Marret, F., Fleitmann, D., Arz, H.W., Nowaczyk, N., Behling, H.,
1252 2013. Eemian and Holocene sea-surface conditions in the southern Black Sea:
1253 Organic-walled dinoflagellate cyst record from core 22-GC3. Mar. Micropal.
1254 101, 146-160.

1255 Sonzogni, C., Bard, E., Rostek, F., Dollfus, D., Rosell-Melé, A., Eglinton, G., 1997.
1256 Temperature and Salinity Effects on Alkenone Ratios Measured in Surface
1257 Sediments from the Indian Ocean. Quaternary Research 47, 3, 344–355.
1258 http://doi.org/10.1006/qres.1997.1885
1259 Sorlien, C.C., Akhun, S.D., Seeber, L., Steckler, M.S., Shillington, D.J., Kurt, H.,
1260 Imren, C., 2012. Uniform basin growth over the last 500 ka, north Anatolian
1261 fault, Marmara Sea, Turkey. Tectonophysics 518, 1-16.
1262 Sorrel, P., Popescu, S.-M., Head, M. J., Suc, J.-P., Klotz, S., Oberhänsli, H., 2006.
1263 Hydrographic development of the Aral Sea during the last 2000 years based on
1264 a quantitative analysis of dinoflagellate cysts, Palaeogeography,
1265 Palaeoclimatology, Palaeoecology 234, 304–327.
1266 Tolun, T., Çağatay, M.N., Carrigan, W.J., 2002. Organic geochemistry and origin of
1267 Holocene sapropelic layer and associated sediments in Marmara Sea. Mar.
1268 Geol. 190, 47–60.
1269 Triantaphyllou, M.V., Antonarakou, A., Kouli, K., Dimiza, M., Kontakiotis, G.,
1270 Papanikolaou, M. D., Ziveri, P., Mortyn, P. G., Lianou, V., Lykousis, V.,
1271 Dermitzakis, M. D., 2009. Late Glacial–Holocene ecostratigraphy of the south-
1272 eastern Aegean Sea, based on plankton and pollen assemblages. Geo-Mar.
1273 Lett. 29, 249–267.
1274 Tudryn, A., Leroy, S.A.G., Toucanne, S., Gibert-Brunet, E., Tucholka, P., Lavrushin,
1275 Y.A., Dufaure, O., Miska, S., Bayon, G., 2016. The Ponto-Caspian basin as a final
1276 trap for southeastern Scandinavian ice-sheet meltwater. Quat Sci Rev 148, 29-43.
1277 Vidal, L., Ménot, G., Joly, C., Bruneton, H., Rostek, F., Çağatay, M.N., Major, C.,
1278 Bard, E., 2010. Hydrology in the Sea of Marmara during the last 23 ka:

Implications for timing of Black Sea connections and sapropel deposition. Paleoceanography 25, PA1205.

Wegwerth, A., Eckert, S., Dellwig, O., Schnetger, B., Severmann, S., Weyer, S., Brüske, A., Kaiser, J., Köster, J., Arz, H.W., Brumsack, H.-J., 2018. Redox evolution during Eemian and Holocene sapropel formation in the Black Sea. Palaeogeography, Palaeoclimatology, Palaeoecology 489, 249–260.

Wegwerth, A., Dellwig, O., Wulf, S., Plessen, B., Kleinhanns, I., Nowaczyk, N.T., Jiabo, L., Arz, H.W., 2019. Major hydrological shifts in the Black Sea “Lake” in response to ice sheet collapses during MIS 6 (130-184 ka BP). Quaternary Science Reviews 219, 126-144.

Yakupoğlu, N., Henry, P., Uçarkus¸ G., Eris, K.K., Demory, F., Crouzet, C., Çağatay, M.N., 2022. Factors affecting thickness and frequency of turbidites triggered by earthquakes in Kumburgaz Basin, Sea of Marmara. Marine Geology 452, 106900.

Yaltırak, C., Alpar, B., Sakınc, M., Yüce, H., 2000. Origin of the Strait of Çanakkale (Dardanelles): regional tectonics and the Mediterranean-Marmara incursion. Mar. Geol. 164, 139-156 (with erratum 167, 189-190).

Yaltırak, C., 2002. Tectonic evolution of the Marmara Sea and its surroundings. Marine Geology 190, 493-529.

Zwiep, K.L., Hennekamp, R., Donders, T.H., van Helmond, N.A.G.M., de Lange, G.J., Sangiorgi, F., 2018. Marine productivity, water column processes and seafloor anoxia in relation to Nile discharge during sapropels S1 and S3. Quaternary Science Reviews 200, 178-190.

Supplementary information

Table SI1: Benthic foraminifera census data in nine samples from core CS22

Core CS22										
benthic foraminifera census data										
	depth (cm)	1631	1632	1915	1935	1955	1975	1995	2015	2035
shallow-water species	*Ammonia parkinsoniana*			2						
	Ammonia sp					1				
	Discorbinella bertheloti							1	3	3
	Elphidium sp			1						
	Haynesina depressula			5						
	Rosalina sp						1		1	2
	Porosononion granosum			1						
hyaline bathyal species	*Amphicoryna scalaris*							1		
	Bolivinita quadrilatera						1			
	Bolivina striatula									2
	Bolivina alata				64	371	101			
	Bolivina dilatata				16	4	5			1
	Bolivina spathulata				1	2	78	9	7	2
	Bulimina aculeata					5	6	8	11	5
	Bulimina inflata					1	4	151	235	115
	Bulimina elongata				7	6	5		1	1
	Bulimina marginata				98	5	1	3	4	1
	Bulimina sp							7	2	
	Cassidulina carinata				15	2	8	32	9	
	Cassidulina obtusa									2
	Chilostomella oolina							2	3	7
	Chilostomella ovoidea					11	10	3		
	Chilostomella sp					3				
	Cibicidoides pachyderma					1	6	35	15	
	Cibicidoides pseudoungerianus							7		1
	Cibicidoides sp						1	8		2
	Dentalina sp								1	
	Fissurina staphylleana							1		
	Globobulimina spp						1		3	
	Globocassidulina oblonga							1	2	8
	Gyroidinoida lamarckiana				1		2	17	10	24
	Gyroidinoida soldanii							1		
	Hyalinea balthica			1	105	9	27	108	8	
	Lagena spp								2	2
	Lenticulina calcar								1	9
	Lenticulina sp				1					
	Melonis affinis				8	1	23	44	3	5
	Melonis pompilioides				8		9	15	9	10
	Neolenticulina variabilis									1
	Nonionella turgida									1
	Planulina ariminensis						20	45	13	35
	Pullenia quadriloba									6
	Robertina sp							1		
	Robertina translucens								1	1
	Saracenaria sp									3
	Siphogenerina columellaris									1
	Siphonina sp									1
	Sphaeroidina bulloides							2		2
	Stainforthia concava				3					
	Uvigerina mediterranea							12		1
	Uvigerina peregrina						4	3	6	7
	Valvulineria bradyana						13	2	11	1
porcelanous species	*Adelosina* sp							1		1
	Articulina tubulosa								1	2
	Biloculinella sp									11
	Comuloculina foliacea								2	
	Pyrgo depressa							1	2	2
	Pyrgo elongata							2		4
	Pyrgoella irregularis						1	2		
	Quinqueloculina padana						2	2	2	11
	Quinqueloculina stelligera						1	2		3
	Quinqueloculina sp								2	8
	Sigmoilopsis schlumbergeri				1		1	1	3	1
	Siphonaperta sp							1		
	Spiroloculina excavata								2	1
	Triloculina tricarinata							2		
	Triloculina sp								1	
	Textularia spp									2
	unidentified species			4	4	1		2	1	2
	total number of counted foraminifera	0	0	14	332	423	331	535	377	310
	total number of shallow water individuals	0	0	9	0	1	1	1	4	5
	total number of bathyal individuals	0	0	5	332	422	330	534	373	305
	BFN (bathyal species only, ind.g^{-1})	0	0	0	386	30	209	277	459	194
	S (number of bathyal taxa)	0	0	1	13	13	24	34	30	40

1304

Table SI2: Ecological assignment of main foraminiferal species in core CS22

Fontanier, F., Garnier, E., Brandily, C., Dennielou, B., Bichon, S., Gayet, N., Eugene, T., Rovere, M., Grémare, A., Deflandre, B. 2016. Living (stained) benthic foraminifera from the Mozambique Channel (eastern Africa): Exploring ecology of deep-sea unicellular meiofauna. Deep-Sea Research I 115, 159–174.

Species adapted to high oxygen conditions (HO)
Cibicidoides spp
Gyroidina lamarckiana
Miliolids excluding *Articulina tubulosa*
Low-oxygen indicators (LO)
Chilostomella spp
Globobulimina spp
Stainforthia concava
Species adapted to high organic fluxes (eutrophic indicators)
adapted to low oxygenation
Bolivina alata
Bolivina dilatata
Bolivina spathulata
not tolerant to low oxygenation
Bulimina marginata
Hyalinea balthica
(after Cornuault et al. 2016 and references therein; Fontanier et al. 2016)

Table SI3: Comparative list of taxa between the Marmara Sea (cores CS22 and CS18) and the SE Black Sea (core 22-GC3; Shumilovskikh et al., 2013).

	CS22	CS18	22-GC3	
	Pyxidinopsis psilata,	Pyxidinopsis psilata,	Pyxidinopsis psilata,	
	Spiniferites cruciformis/Galeacysta etrusca,	**Spiniferites cruciformis/Galeacysta etrusca,**		VV
		Galeacysta etrusca,		0
	S. cruciformis A,	S. cruciformis A,	S. cruciformis,	
	S. cruciformis B,	S. cruciformis B,	S. cruciformis,	
	S. cruciformis C,	S. cruciformis C,	S. cruciformis,	
		Pterocysta cruciformis,		0
	S. inaequalis,	**S. inaequalis,**		VV
		Romanodinium areolatum,		0
		Caspidinium rugosum,	Caspidinium rugosum,	
		C. rugosum rugosum,		only in MIS6
		Impagidinium sp. A,		only in MIS6
6/13		**I. caspienense,**		0
	Lingulodinium machaerophorum ss,	Lingulodinium machaerophorum ss,	Lingulodinium machaerophorum,	
		L. machaerophorum B,		0
1/3		**L. mach. bulbous,**		0
		Dubridinium caperatum,	Dubridinium caperatum,	
		Lejeunecysta marieae,		0
			Lejeunecysta sabrina?	0
			Quinquecuspis sp.	0
			Quinquecuspis concreta	VV
	Votadinium calvum,	Votadinium calvum,	Votadinium calvum,	
	Brown baggy cyst,	Brown baggy cyst,	Brigantedinium sp.	
			B. cariacoense	V
			B. simplex	V
			C. Gymnodinium microret./nolleri	0
	Xandarodinium xanthum,	Xandarodinium xanthum,	Xandarodinium xanthum,	
	C. Protoperidinium nudum,	C. Protoperidinium nudum,	C. Protoperidinium cf nudum	
		C. Protoperidinium stellatum,	C. Protoperidinium stellatum,	
	C. Polykrikos hartmanii,	**C. Polykrikos hartmanii,**		0
			C. Polykrikos schwartzii	0
			Echinidinium sp.	0
5/8			**E. zonneveldiae**	0
	S. belerius,	S. belerius,	S. belerius,	
	S. bentorii,	S. bentorii,	S. bentorii,	
			S. bulloideus	0
	S. elongatus,		S. elongatus,	
	S. hainanensis,			V
			S. hyperacanthus	VV
			S. membranaceus	VV
	S. ramosus,	S. ramosus,	S. ramosus,	
	S. septentrionalis,	S. septentrionalis,	S. septentrionalis,	
	Spiniferites sp.,	Spiniferites sp.,	Spiniferites sp.,	
	S. mirabilis,	S. mirabilis,	S. mirabilis,	
	S. pachydermus,		S. pachydermus,	
	Polysphaeridium zoharyi,	**Polysphaeridium zoharyi,**		VV
	Tuberculodinium vancampoae,	Tuberculodinium vancampoae,	Tuberculodinium vancampoae,	
	Operculodinium israelianum,	Operculodinium israelianum,		0
	O. centrocarpum,	O. centrocarpum,	O. centrocarpum,	
	Ataxodinium choane,	Ataxodinium choane,	Ataxodinium choane,	
	Bitectatodinium tepikiense,	Bitectatodinium tepikiense,	Bitectatodinium tepikiense,	
	Tectatodinium pellitum,	Tectatodinium pellitum,	Tectatodinium pellitum,	
	C. Pentapharsodinium dalei,	C. Pentapharsodinium dalei,	C. Pentapharsodinium dalei,	
		C. Alexandrium sp.,		0
	C. Scrippsiella trifida,	**C. Scrippsiella trifida,**		VV
	Pyxidinopsis reticulata,			0
21/17	Nematosphaeropsis labyrinthus,	Nematosphaeropsis labyrinthus,	Nematosphaeropsis labyrinthus,	
			Achomosphaera cf andalousiense	VV
	33	41		
				0 = insignificant
				V = different
				VV = very different

1317

1318

22 March 2023

We have no competing interests

Dinocyst assemblages and water surface conditions in the Sea of Marmara during MIS 6 and 5 from two long cores

Leroy S.A.G. [1-2-3-*], Henry P. [1], Marret F[3], Pailles C. [1], Licari L. [1], Kende J. [1], Rostek F. [1], Bard E. [1]